Hochschule Neubrandenburg
University of Applied Sciences

GEOMAGNETICALLY INDUCED CURRENTS IN THE GERMAN POWER GRID

ALINE GUIMARÃES CARVALHO

Master of Engineering (M.Eng.)
Faculty of Geodesy and Geoinformatics
Hochschule Neubrandenburg

First Supervisor: Prof. Dr.-Ing. Andreas Wehrenpfennig
Second Supervisor: Dr. Leonie Pick

May 2023

URN: urn:nbn:de:gbv:519-thesis2023-0002-7

Neubrandenburg

ABSTRACT

Geomagnetic storms are widely recognized to affect and threaten technological systems on the Earth's surface. Geomagnetically induced currents (GICs) result from the geoelectric field induced in the Earth's conductive subsurface under conditions of intense geomagnetic disturbance (GMD) and, when in contact with grounded power systems, have the potential to generate harmonics that can lead to transformer failure and damage other components of the grid. GICs have been an important research topic in various countries for decades, especially in countries located at high latitudes. In recent years, however, it has been shown that GICs pose a threat also to mid-latitude countries. In the case of Germany, a comprehensive overview of how the GICs may affect the power grid is not yet fully developed.

In this context, this study aims to model the GICs in the German high-voltage transmission grid, which is the part of the power system mainly affected by these currents. The GIC calculations are generally divided into two parts: the geophysical part, which aims at estimating the induced geoelectric field from the GMD input, and the engineering part, which is related to the calculation of the current flowing in the electric grid based on the estimated geoelectric field.

The network modeling (engineering part) is the focus of this study. In the first part of this investigation, the calculation of the GICs is performed for a section of the power grid in northwestern Germany for a time period in February 2016. The modeling results are then compared to transformer neutral point measurements from a substation located in the same grid section and time period. The measurements are also used to calculate coefficients that describe the network and allow the fitted model to be applied. The developed model allows the calculation of the GICs for different power grids in any time period.

In order to develop the network model, publicly available sources are used to obtain the electrical properties of the grid. For the cases where no public information is available, assumptions based on the literature have been adopted. In the second part of this work, the model is applied to the 2003 Halloween Storm to calculate the GICs on the grid section for an extreme spatial weather event.

The results indicate a good outcome for the GIC modeling with the available parameters and the approach employed. However, updated measurements would help to increase the reliability of the modeling, as well as more detailed information about the network topology since it greatly influences the GICs flowing into the grid.

ACKNOWLEDGMENTS

I would like to express my most sincere gratitude to my supervisors, Prof. Dr.-Ing. Andreas Wehrenpfennig, who gave me valuable support during my studies and provided all the necessary guidance for completing this work, and Dr. Leonie Pick, who, with her experience and knowledge, guided me into the scientific world, always encouraging and inspiring me.

I am also grateful to all the colleagues in the Effects on technical systems group and all the colleagues from DLR, who somehow contributed to this work and made the working environment friendly and welcoming. Working at DLR has been a valuable and positive experience, which I greatly appreciate.

I extend my gratitude to Michael Schühle and Prof. Dr.-Ing. Stefan Tenbohlen for their contribution with previous studies and information on the topic. I acknowledge Amprion GmbH for their collaboration.

There are no words to express my gratitude to my family. I especially want to thank my parents, Valdenir Bezerra Guimarães and Waltan Ramos de Carvalho, and my husband, Arthur Amaral Ferreira, who always believed in me and supported me.

Finally, I acknowledge the work of André Miede and Ivo Pletikosić, whose LATEX model was used for compiling this thesis.

CONTENTS

LIST OF FIGURES

LIST OF TABLES

LIST OF SYMBOLS

Sign	**Description**	**SI unit**
B	Magnetic field	T
C	Capacitance	F
E	Electric field	$V \cdot m^{-1}$
f	Frequency	Hz
G	Conductance	S
I	Electric current	A
L	Inductance	H
R	Electrical resistance	Ω
V	Voltage	V
X	Electrical reactance	Ω
Y	Admittance	S
Z	Electrical impedance	Ω
μ	Permeability	$H \cdot m^{-1}$
μ_0	Magnetic permeability of free space	$H \cdot m^{-1}$
ω	Angular frequency	$rad \cdot s^{-1}$
ϕ	Magnetic flux	Wb

ACRONYMS

AC alternating current

DC direct current

ESA European Space Agency

G-ESC Geomagnetic Conditions Expert Service Centre

GMD geomagnetic disturbance

GICS geomagnetically induced currents

HVDC high-voltage direct current

KCL Kirchhoff's current law

NOAA National and Atmospheric Administration

NSTC National Science and Technology Council

SO Solar-Terrestrial Physics

SWPC Space Weather Prediction Center

SWE Space Weather Services Network

TSOS transmission system operators

1 INTRODUCTION

1.1 THE GERMAN POWER GRID AND SPACE WEATHER

The electric power industry, as known today, was first established by Thomas A. Edison as he inaugurated the first known electricity generating station, Pearl Street Station in New York City in 1882. The station was responsible for supplying 110 V incandescent lighting to 59 customers over a 2.5 square kilometer area, totaling a load of 30 kW, provided at that time by direct current (DC) generators (Glover et al., 2022).

The power industry experienced significant growth in the following years, as did the need for electricity, and so there was an increase in loads and transmission distances. The expansion was, however, limited by voltage-related challenges, as there were large voltage drops along the transmission lines, as well as power losses. The development of the first practical transformer by William Stanley in 1885, along with the alternating current (AC) system, changed the way power was transmitted, as it enabled the changing of the voltage level in order to transmit power with a lower current. The advantages of AC and polyphase systems were soon recognized and spread. In 1891 Germany brought its first three-phase line into operation, capable of carrying power at 12 kV over 179 km (Glover et al., 2022).

Nowadays, the German transmission network comprises a total length of about 35,000 kilometers, including extra-high voltage lines up to 220 kV and 380 kV. Most power lines work with AC, although new transmission lines using high-voltage direct current (HVDC) are planned to be completed by 2025 to link northern and southern Germany. Four transmission system operators (TSOs) are responsible for keeping the grid safe and stable: Amprion, TenneT, TransnetBW, 50Hertz. Each of them operates the network in different areas across the country (Appunn and Russell, 2021). The map in Figure 1.1 indicates the area of operation for each of the four TSOs.

With the growing demand for electricity and the importance of a reliable supply, there has been an increasing need to consider renewable sources for energy generation. Germany plans to reduce its dependence on fossil fuels, thereby reducing CO_2 emissions while phasing out nuclear power plants. The program known as *Energiewende* has been implemented in recent years and aims to have 65% of the country's total demand supplied by renewable energy sources by 2050. In 2021, Germany had a total net public electricity generation of 495 TWh, of which about 46% came from renewable sources – 22.6% from wind power (on-shore and off-shore) (Appunn, 2021). One of the challenges encountered during this process is the extensive distance between the main load centers, located mainly in the southern and western parts of the country, and the on-shore and offshore wind generation resources, located mainly in the north. A significant improvement of the

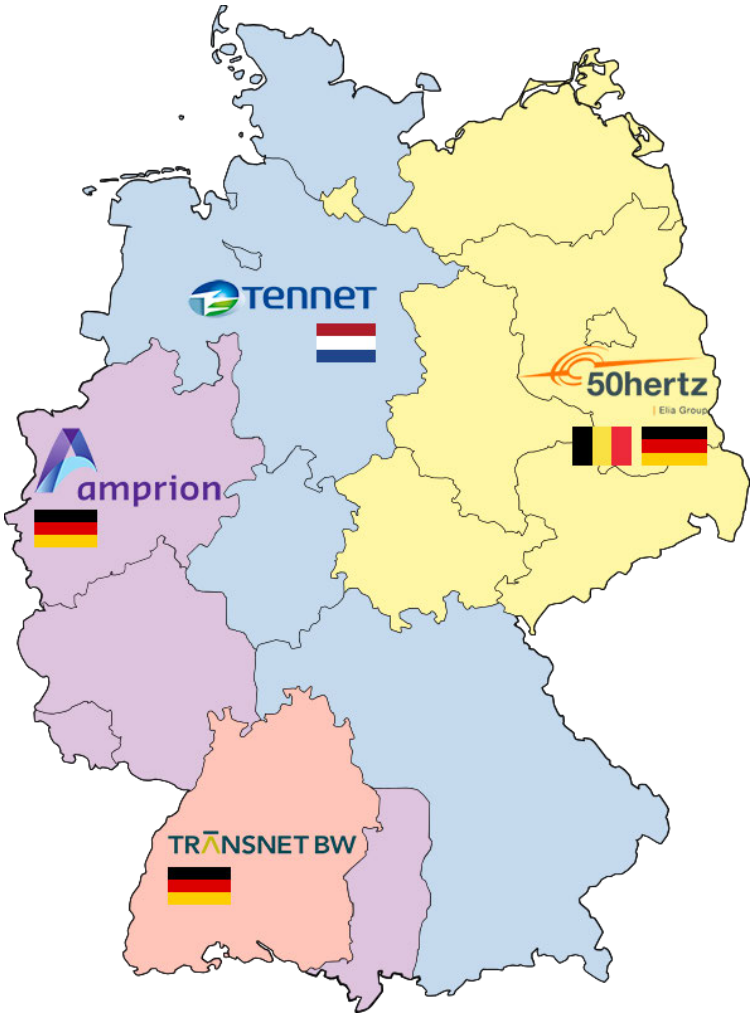

Figure 1.1: Map of Germany divided by regions of operation for the four TSOs (McLloyd, 2020).

existing transmission infrastructure has been necessary to successfully implement the *Energiewende* (Schönleber et al., 2020).

Along with the modifications to the power grid, new challenges arise. It is then necessary to draw attention to different aspects of the network since the system must be able to respond to problems that could compromise its operation. Power failures have negative consequences and can have large economic impacts; therefore, possible threats must be anticipated and considered when building the grid.

Although the structure itself is a crucial aspect to consider when it comes to the reliability and safety of the power grid, many of the components of the network are exposed to the weather. Therefore, weather conditions have the potential to impact the supply of electricity. Severe storms, strong winds, lightning, heavy snow, and high temperatures are examples of weather changes that can be responsible for producing faults in grid systems, which can lead to undesirable consequences on a large scale and affect the power supply (Ward, 2013).

In addition to the typical weather changes, the disturbances related to space weather, which refers to the conditions in space between the Sun and Earth that vary

continuously, also need to be considered. Among the disturbances, geomagnetic storms can pose a significant threat to the power grid system. Geomagnetic storms describe a global, characteristic disturbance of the Earth's magnetic field in response to solar eruptions transmitted through interplanetary space by the solar wind. These disturbances have the potential to generate geomagnetically induced currents (GICs), which are quasi-DC and flow through any ground-based, elongated, and electrically conducting parts of critical infrastructure, such as overhead lines, pipelines, and railways, and can cause disruptions and damage to these systems (Gonzalez et al., 1994).

It is recognized that the power grid is the most critical structure affected by GICs, mainly because today's society is highly dependent on it. The study of GICs is of great complexity, especially considering the interdisciplinary nature of the topic as it involves understanding solar physics, space weather, geophysics, and power engineering (Gannon, Swidinsky, and Xu, 2019). The risk assessment of GICs on the power grid can be divided into three parts: the hazard, the grid exposure, and the grid vulnerability (Ngwira and Pulkkinen, 2019). The first is related to the induced geoelectric field, as higher values of the induced geoelectric field lead to a higher GIC hazard. The electric field depends on the intensity and orientation of the geomagnetic disturbance and the ground conductivity structure. The conductivity structure varies according to the local geology, while the intensity and orientation of the geomagnetic disturbance are associated with space weather conditions. Large geomagnetic disturbances are typically observed at high latitudes, making the geoelectric field larger in areas near the auroral zone (Molinski, 2002).

The exposure of the grid depends on the network's characteristics, mainly related to the lines and the grounded components. The voltage level also has an impact, as does the length of the lines and their orientation. The vulnerability of the grid is related to the capability of the grid to cope with additional DC currents. DC currents mainly affect transformers due to half-cycle saturation and have the potential to create harmonics, which can be harmful to grid operation. According to Beltle, Schühle, and Tenbohlen, 2017, a DC current of 100 mA is already enough to produce saturation in transformers.

Over time, there have been several occasions when geomagnetic storms have caused damage to power network infrastructures. One of the most widely known occurred in 1989 in Quebec, where GICs caused a 9-hour blackout (Winter, 2019). As it was believed that GICs would only affect countries near the poles, past studies focused on high latitudes. However, recent events (e.g., the 2003 Halloween storm) have increased the attention to other regions, and it was found that geomagnetic storms could have effects at much lower latitudes. Investigations have been conducted at mid and low latitudes (e.g., Bailey et al., 2017), and it has been proven that not only high-latitude countries are at risk of GICs, as previously thought, but also lower latitudes can be significantly impacted by high geomagnetic activity.

Space weather has attracted the attention of international entities and governments. In the US, the National Science and Technology Council (NSTC), through the National Space Weather Strategy and Action Plan, has developed strategies to act on activities to improve the country's preparedness for space weather events (Council, 2019). In addition, the Space Weather Prediction Center (SWPC) of the

National and Atmospheric Administration (NOAA) provides products that describe the space environment, such as the geomagnetic activity forecast for the next three days and near real-time electric field mapping for the United States (SWPC, 2023). In Europe, the Space Weather Services Network (SWE) from the European Space Agency (ESA) created the Geomagnetic Conditions Expert Service Centre (G-ESC), which develops products related to geomagnetic field variations and already provides relevant information for the assessment of the GIC in different countries (not yet in Germany; ESA, 2023).

The hazard that GICs may pose to the German power grid is still unclear, as not many studies have been conducted in this region. Thus, it is of great importance to investigate the impacts that extreme spatial weather events could have on the German power transmission network. The Institute for Solar-Terrestrial Physics (SO) is engaged in space weather research, with the aim to protect national infrastructures and support impacted sectors based on reliable, accurate, and timely observations and forecasts (DLR, 2023). This master's thesis was written in the framework of the research conducted at the group Effects on technological systems, which is part of the Department for Space Weather Impacts (WWE) and investigates relevant effects of space weather on technical infrastructure.

1.2 OBJECTIVES AND STRUCTURE OF THE THESIS

This study aims to model the GICs in the German power grid, and for this purpose, a case study in 2016 is considered. In this case study, GICs are calculated at the neutral of transformers for a grid section in the north-western part of Germany; the results are then compared to measurements published on Schühle and Tenbohlen, 2020. After that, the model is applied to calculate the GICs in the same power grid section for the Halloween Storm in 2003, and the results are compared to the GIC modeled using the system parameters determined from the measurements (modeling based on Pulkkinen, Pirjola, and Viljanen, 2007).

In order to be able to model GICs, it is necessary to understand the characteristics of the power grid. Therefore, Chapter 2 describes the power grid in the context of GIC modeling, including transmission lines and transformers as the most relevant components for this subject. Chapter 3 then presents an overview of space weather and how it affects the power grid, including examples of important extreme space weather events. Chapter 4 details the procedure used to model GICs, starting from the geoelectric variations caused on Earth by a geomagnetic storm and reaching down to the computation of the GIC at the neutral of transformers in the power grid. Finally, the grid section modeling is described in Chapter 5, with details on which parameters were considered. The results of the 2016 case study and the Halloween Storm are also presented in this chapter and further discussed in Chapter 6. The conclusions of the work are drawn in Chapter 7.

2

POWER GRID DESCRIPTION

A good understanding of the power grid and of the most important aspects to consider when calculating GICs is essential in order to be able to model the GIC originated by a geoelectric field. In this regard, this Chapter presents an overview of the parameters required for modeling the power grid in the context of GIC calculation, starting by describing the transmission lines, transformers, and their equivalent circuits. Given the importance of transformers for GIC analysis, their magnetization characteristic and the impact that a DC current represents for their operation are also discussed, along with the different types of winding connections considered for GIC modeling. Finally, the derivation of the $\boldsymbol{Y_{BUS}}$ matrix is performed, which is a matrix that characterizes the power system and facilitates the calculation of voltages and currents at any point of the grid.

The electric power system network is designed to transfer electrical energy from generation centers to the final consumers. It can be divided into three main sectors: generation, transmission and distribution (Fang et al., 2012). Figure 2.1 exemplifies a typical electric power system.

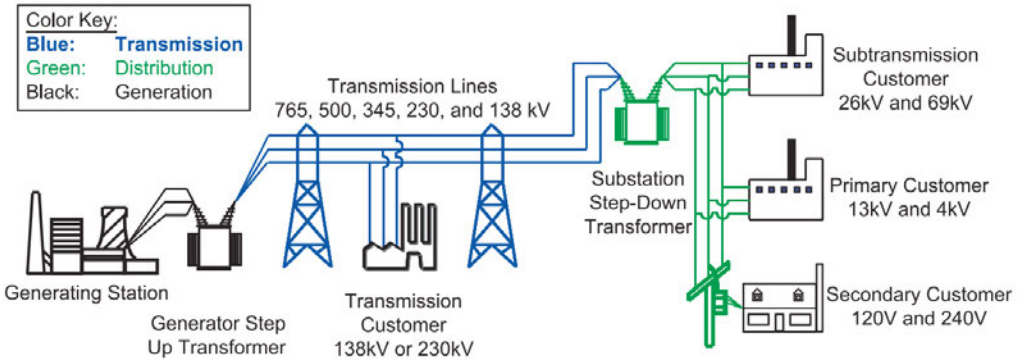

Figure 2.1: Electric power system (U.S.-Canada Power System Outage Task Force, 2004).

Electricity is generated in power plants, usually at voltage levels between 11 kV and 33 kV. As power plants are often located far from consumers, electrical power may need to travel long distances, in some cases up to hundreds (or even thousands) of kilometers, and, as a consequence, a large amount of energy is likely to be lost due to heat dissipation through the conductors (Singh, 2008).

In order to minimize energy loss during the transmission process, step-up transformers are used to increase the voltage level, enabling transmission to be carried out at high and extra high voltages, typically ranging from 110 kV-1000 kV. Closer to the consumption centers are substations with step-down transformers, lowering the voltage levels to be appropriate for use by industrial, commercial, or residential customers (Alcayde-Garcia et al., 2022).

When it comes to geomagnetic storms and the resulting GICs, previous studies have proven that higher voltages are more susceptible to these disturbances, as

high-voltage lines have smaller resistances (based on Ohm's law; see Eq. 4.3; Zheng et al., 2014). For this reason, this work focuses on the transmission power grid, specifically at voltage levels of 200 kV and above. The following section presents a description of transmission lines.

2.1 TRANSMISSION LINES

Transmission lines can carry alternating or direct current and consist of overhead or underground lines. The transmission system worldwide is, even so, predominantly composed of overhead lines, which are most commonly AC and three-phase. Overhead transmission lines comprise conductors, insulators, support structures, and shield wires (Glover et al., 2022).

The fundamental parameters for modeling a transmission line are series resistance, series inductance, shunt capacitance, and shunt conductance. Each parameter accounts for a different effect on the line when electrical power is flowing, and depending on the purpose of the modeling, it is possible to neglect one or more effects (Glover et al., 2022).

The physical operation of a transmission line changes depending on its length, so the representation of the circuit differs in terms of whether the line is short, medium or long. Typically, medium-length lines range from 25 to 250 km and can be represented by the so-called nominal π circuit, as in Figure 2.2.

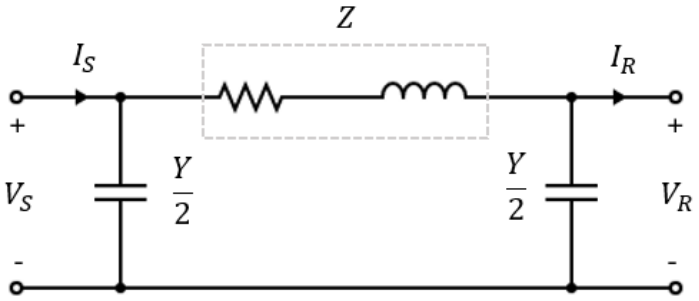

Figure 2.2: Nominal π circuit. Adapted from Glover et al., 2022.

The parameters represented in Figure 2.2 refer to the total series impedance and the total shunt admittance (Z and Y, respectively). V_S and I_S are the sending-end voltage and current, and V_R and I_R are the receiving-end voltage and current (Glover et al., 2022).

The total series impedance and total shunt admittance can be described as $Z = (R + j\omega L)l$ [Ω] and $Y = (G + j\omega C)l$ [S], where R, L, G and C are the resistance, inductance, conductance and capacitance, respectively. l is the line length and $\omega = 2\pi f$ is the angular frequency for the power system nominal frequency f (50 Hz in Europe; Glover et al., 2022).

For overhead lines, the shunt conductance (G) is normally neglected. Moreover, as the main objective of this work is the modeling of the GICs, which are considered quasi-DC, only the DC components of the system are of interest, so L and C are also neglected. Thus, for the purpose of calculating GICs, the total shunt admittance

can be ignored, and a transmission line can be represented by its total series resistance (R) (Zheng et al., 2014). The next section presents a description of power transformers, including the most relevant aspects when modeling GICs.

2.2 TRANSFORMERS

Transformers are static devices constructed by two or more windings and a common magnetic core, usually made of iron or steel. They are essential components for the efficient operation of the power grid, due to their mechanism of transferring electrical power from one circuit to another without modifying the frequency while changing voltage and current levels (Allan and Moore, 2004).

The operation of a transformer works on the basis of Faraday's law of induction, which states that a time-varying magnetic flux linked with a circuit will induce a voltage in the circuit proportional to the rate of change of flux (Witulski, 1993).

Figure 2.3 represents a single-phase two-winding transformer, where N_1 and N_2 are the number of turns in the primary and secondary windings, while E_1 and E_2 are the voltages across the windings (Glover et al., 2022). When an AC voltage is applied to the primary winding terminals, a current (I_1) will flow through it and produce a varying flux in the magnetic circuit. The flux then induces a voltage in the secondary winding, which results in a current (I_2) that flows in the secondary winding when a load is connected to its terminals, forming a closed path (Witulski, 1993).

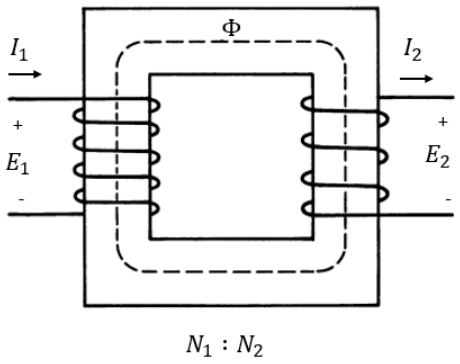

Figure 2.3: Two-winding power transformer. Adapted from Daniels, 1976.

The basic relations for an ideal single-phase two-winding transformer can be written as

$$\frac{E_1}{E_2} = \frac{N_1}{N_2} \tag{2.1}$$

and

$$\frac{I_1}{I_2} = \frac{N_2}{N_1}. \tag{2.2}$$

It is assumed that ideal transformers have no core losses or losses in the windings, zero core reluctance and no leakage flux (Glover et al., 2022). For a better understanding of the operation of power transformers and how they are included in the power grid, the following sections provide a circuit representation of the single-phase two-winding transformer, the magnetization characteristic curve of transformers, and the three-phase connections most relevant to GIC modeling.

2.2.1 *Equivalent circuit*

In practice, the process of transferring power through a transformer is not lossless and the corresponding losses need to be considered. Figure 2.4 illustrates the equivalent circuit of a practical two-winding transformer. E_1 and E_2 refer to the voltages across the primary and secondary windings, respectively, while V_1 and V_2 are the voltages at the primary and secondary terminals of the transformer. I_1 and I_2 correspond to the currents at the primary and secondary terminals.

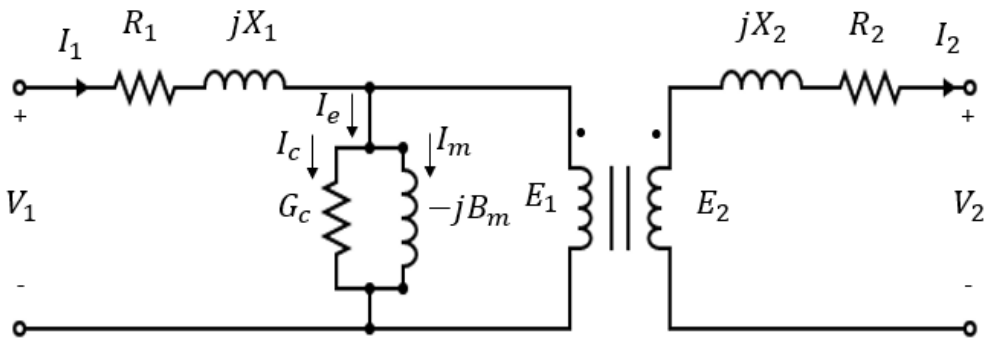

Figure 2.4: Equivalent circuit of two-winding power transformer (Glover et al., 2022).

The windings of a transformer have resistances, which correspond to the Joule heating losses and are represented in series with the windings as R_1 and R_2. The magnetic flux in practice exists not only within the core. Instead, each of the windings has a flux component, known as the leakage flux, that is not connected to the other. The leakage flux is represented by the reactances X_1 and X_2, which account for the reactive power losses (Glover et al., 2022).

Hysteresis and eddy current losses are present in the core and are represented by the conductance G_c, which carries the core loss current (I_c). In addition, reactive power is needed to magnetize the core and is represented by the susceptance B_m, which is associated with the magnetization current (I_m). Both G_c and B_m together will form the shunt branch, in which the exciting current (I_e) flows (Glover et al., 2022).

The exciting current is typically very small compared to the rated current of the transformer, so the shunt branch is often dropped out. Thus, a transformer can be represented only by the resistance and reactance of the series windings.

Considering that only the DC components are of concern for GIC studies, only the real part, i.e., the resistance, is considered.

2.2.2 *Magnetization Characteristic*

The magnetization curve (B-H) represents the relationship between the magnetic flux density B and the magnetizing force H, which is given by $B = \mu H$ for ideal transformers, where μ is the core permeability. In order to minimize the losses in the transformer core, ferromagnetic materials with high permeability are used. In practice, the B-H relation is non-linear and multivalued and changes according to the material. The black curve in Figure 2.5 illustrates the B-H curve. The curve can be divided into three parts: the linear, knee, and saturation regions. A well-designed transformer is built to operate in the knee region (see point A_1 in Figure 2.5; Glover et al., 2022).

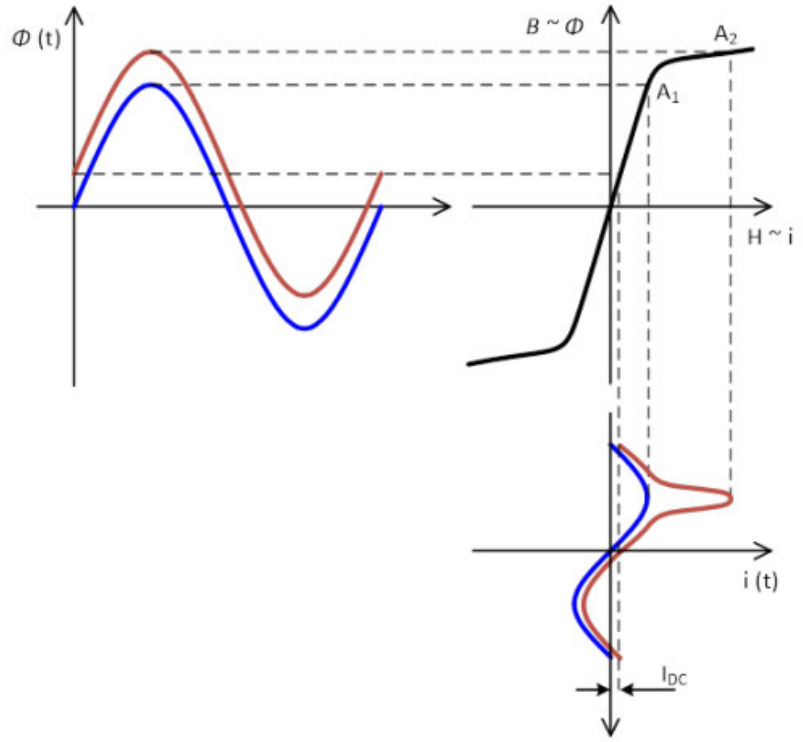

Figure 2.5: Magnetization core behavior. The black curve is the magnetization curve (B-H). The curves in red represent normal operation, while the curves in blue show the changes in the case of a superimposed DC current (I_{DC}; Beltle, Schühle, and Tenbohlen, 2017).

In the case of an additional DC current being injected into the transformer, a direct magnetic force is generated as a consequence of Ampere's law. The presence of this additional magnetic force results in a shift of the working point of the transformer along the magnetic characteristic curve (point A_2 in Figure 2.5). A constant magnetic flux ϕ_{DC} is then generated (Beltle, Schühle, and Tenbohlen, 2017).

When an alternating magnetic flux ϕ_{AC} produced by an alternating voltage already exists in the transformer, the constant and alternating fluxes superimpose, and saturation occurs. Once the core is saturated, its material becomes inefficient, and the coil behaves like a coil of air. As a consequence, the magnetizing current increases rapidly. As the DC only brings the operating point to saturation for a half-cycle of the period, this effect is known as half-cycle saturation. Small DC currents in the range of 100 mA can already trigger it (Beltle, Schühle, and Tenbohlen, 2017).

2.2.3 *Three-phase connections*

There are four ways of connecting the windings of a three-phase transformer: Y-Y (Wye-Wye), Y-Δ (Wye-Delta), Δ-Y (Delta-Wye) and Δ-Δ (Delta-Delta) (Glover et al., 2022). The Wye connection has a neutral point (N), which is the symmetry point and may or may not be grounded. When grounded, the connection is called GWye, as in grounded-wye. Grounding is done through the effective grounding resistance (R_G), which is the equivalent resistance in series of the substation's grounding resistance and the transformer's neutral resistance, if one exists (Shetye and Overbye, 2019).

For GIC calculations, all grounded connections need to be considered. The GWye-GWye type transformers are widely used in transmission systems. The grounding of the neutral is usually included for safety purposes. Also relevant is the autotransformer. In this type of configuration, the two windings are connected in series such that they are coupled both electrically and magnetically. Figure 2.6 shows the different winding connections for three-phase transformers considered for GIC modeling (Shetye and Overbye, 2019).

Delta-Wye connections are typically present in generator step-up transformers. They have the advantage of trapping the third harmonic magnetizing current within the delta winding, which is generated when the transformer core operates in the saturated region of the B-H curve (Glover et al., 2022). GICs do not flow on the delta side of these transformers, since they are not grounded. For the same reason, delta-delta transformers are not considered for GIC modeling, as their configuration has no neutral point (Shetye and Overbye, 2019).

2.3 ADMITTANCE MATRIX $\boldsymbol{Y_{BUS}}$

Sparsing techniques are widely employed to solve the power flow problem for power systems. To simplify the solution, large systems are usually described as a network of admittances, using the nodal admittance matrix ($\boldsymbol{Y_{BUS}}$), which consists of a matrix of size NxN for a system with N buses, where bus has the same meaning as node (Boteler and Pirjola, 2017).

Admittance is the inverse of the impedance, $Y = \frac{1}{Z}$. The diagonal elements of the $\boldsymbol{Y_{BUS}}$ contain the so-called self-admittances, which correspond to the sum of all admittances connected to one bus k. The off-diagonal elements are called the mutual admittances, which are the negative of the admittances between two nodes k and n. The elements of the matrix can then be calculated as,

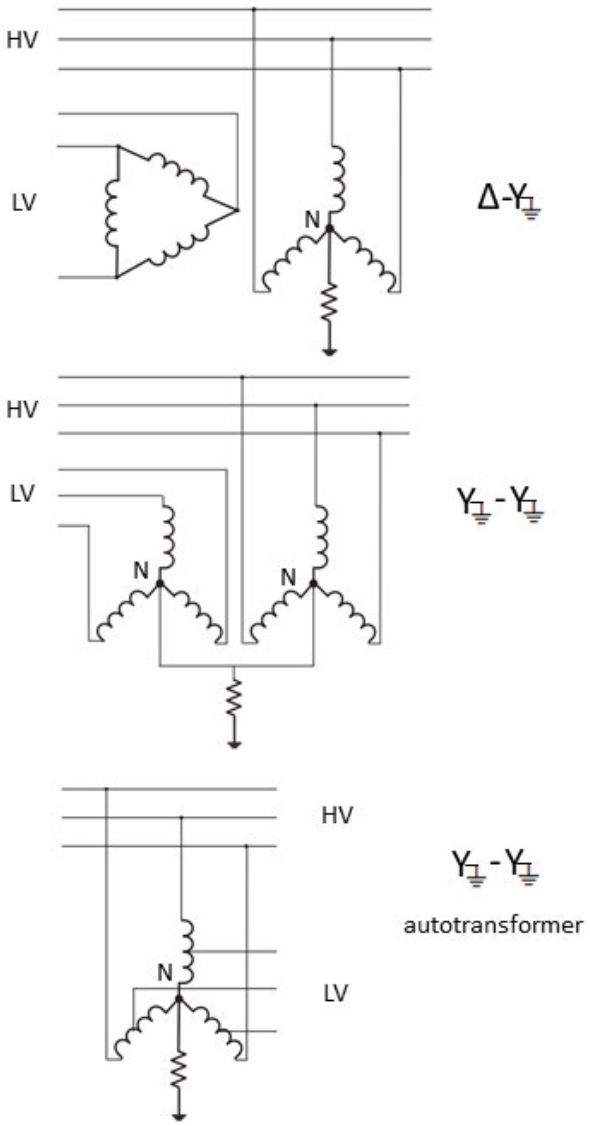

Figure 2.6: Winding connections for three-phase transformers, where HV stands for high-voltage and LV for low-voltage. From top to bottom: Delta-GWye, GWye-GWye and GWye autotransformer. Adapted from Torta, Marsal, and Quintana, 2014.

$$\begin{cases} Y_{kk} = y_k + \sum_{n=1}^{N} y_{kn} \quad n \neq k \\ Y_{kn} = -y_{kn} \end{cases} \tag{2.3}$$

Here the lowercase y's represent the admittances connected to each bus, in order to distinguish them from the matrix components, represented by the uppercase y's. The $\boldsymbol{Y_{BUS}}$ matrix is usually very sparse, due to the fact that in large systems many buses are not connected to each other. The voltage at each bus can thus be determined by applying nodal analysis, using Kirchhoff's current law (KCL) and Ohm's law as follows,

$$\begin{bmatrix} Y_{11} & Y_{12} & Y_{13} & \cdots & Y_{1N} \\ Y_{21} & Y_{22} & Y_{23} & \cdots & Y_{2N} \\ Y_{31} & Y_{32} & Y_{33} & \cdots & Y_{3N} \\ \vdots & \vdots & \vdots & \ddots & \vdots \\ Y_{N1} & Y_{N2} & Y_{N3} & \cdots & Y_{NN} \end{bmatrix} \begin{bmatrix} V_{10} \\ V_{20} \\ V_{30} \\ \vdots \\ V_{N0} \end{bmatrix} = \begin{bmatrix} I_1 \\ I_2 \\ I_3 \\ \vdots \\ I_N \end{bmatrix} \tag{2.4}$$

or,

$$\boldsymbol{V} = \boldsymbol{Y_{BUS}^{-1}} \boldsymbol{I}. \tag{2.5}$$

In order to use the above equations for determining the voltages at each bus, all power sources present in the power system need to be expressed in the form of current sources. Such that, the source of current injected at each bus, that is, the variables of the current vector on the right-hand side of the equation 2.4, are known. Once the voltages at each bus are determined, the current flowing through any component of the network can be found.

This Chapter has presented an overview of the power grid and the components relevant for the calculation of GICs. In this context, the power network can be modeled using the equivalent circuit for transmission lines and transformers. Due to the quasi-CD nature of the GICs, only the real part of each component is considered; therefore, the final network will contain only resistances and energy sources. The energy sources come from the geomagnetic storms and are included in the model in the form of injected currents, and thus $\boldsymbol{Y_{BUS}}$ can be used to calculate the voltage at all nodes. Finally, after the voltages are known, the GIC derived from the GMDs can be computed for any point in the network on the basis of Ohm's law.

The next Chapter will introduce space weather and elaborate on how GICs arise on Earth due to geomagnetic storms, as well as their possible impacts on the power grid. More details regarding the grid modeling and calculation of GICs can be found in Chapter 4.

3

GEOGMAGNETICALLY INDUCED CURRENTS (GICS)

This chapter addresses space weather and describes how solar activity reaches Earth, creating geomagnetic disturbances and subsequently GICs on grounded systems, including electrical power systems. Factors that influence and increase the susceptibility of GICs with high magnitudes are highlighted. In the following sections, the effects that GICs potentially cause on the power grid infrastructure are described and the most extreme space weather events known to have occurred to date are outlined.

Space weather is concerned with the changes constantly occurring in the space environment between the Sun and the Earth. Charged particles are emitted by the sun, forming the solar wind, which carries these particles toward Earth (Gonzalez et al., 1994). Upon reaching the Earth, an exchange of energy and momentum takes place between the solar wind and the coupled magnetosphere-ionosphere system. Following a solar eruption, in which this exchange is sporadically enhanced causing a characteristic distortion of Earth's magnetic field. This geomagnetic disturbance (GMD) is known as a geomagnetic storm (Gonzalez et al., 1994). The global field distortion is equivalent to the appearance of intense, large-scale electric currents in the magnetosphere-ionosphere system, whose presence is imprinted in the temporal variation of the ground-based magnetic field. A geoelectric field will also be induced, as states Faraday's law of induction. When the electric field is induced nearby ground-based, conducting technological networks, geomagnetically induced currents (GICs) will flow. Figure 3.1 shows the space weather chain, starting with the solar activity and ending with GICs. Some examples of the affected ground-based networks are: electric power systems, gas and oil pipelines, railway equipment and telecommunication cables (Bothmer and Daglis, 2007).

GICs are considered quasi-DC, as their frequencies are very small ($\leq$ 1 Hz) compared to the grid nominal frequency (50 Hz). They are driven by induced voltages on the transmission lines and flow through the grounded neutrals of transformers present in power systems (Molinski, 2002). Figure 3.2 illustrates the flow of GICs in a three-phase power system. The main factors that influence the modeling of the GIC are the geoelectric field and the characteristics of the power system. The geoelectric field on the Earth's surface depends on the ground magnetic field variations (dB/dt) and the subsurface conductivity structure (Pulkkinen, Pirjola, and Viljanen, 2007).

The susceptibility to GICs is variable depending on geographic location. Initially, studies on GICs used to focus on high-latitude regions, due to the greater geomagnetic variations present in the vicinity of the auroral oval. In recent years, interest in studying the impacts of GICs in mid- and low-latitude regions has increased, as it is now acknowledged that these regions may also be threatened as the auroral oval expands equatorward during geomagnetic storms (Bailey et al., 2017). Furthermore, as stated above, not only the geomagnetic variation impacts the magnitude of GICs. For instance, coastal areas are highly susceptible to GICs due to the difference in

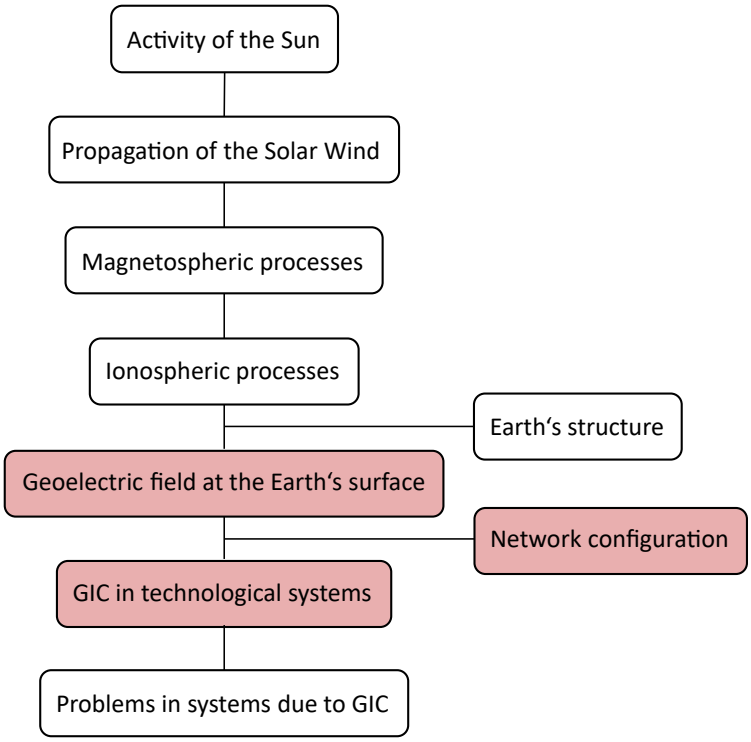

Figure 3.1: GIC chain (Pirjola, 2000). The steps in red are covered by this work.

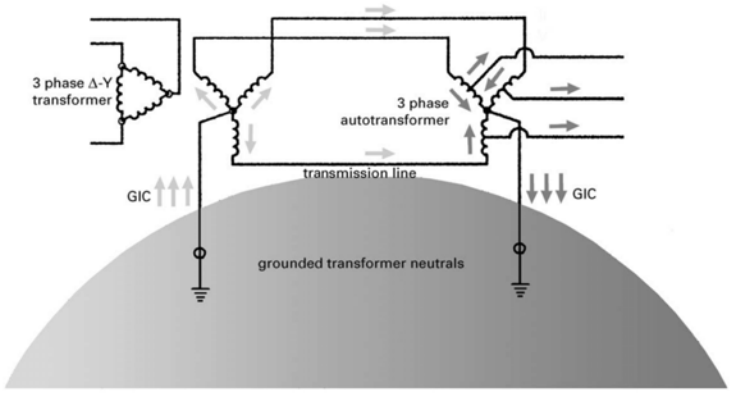

Figure 3.2: GIC flow in a three-phase power system (Molinski, 2002).

resistance between the ocean and the land, so that the induced current coming from the ocean encounters greater resistance when entering the land (Molinski, 2002). The electrical conductivity structure is an important factor in the calculation of GICs, as it affects the induced geoelectric field so that low ground conductivity increases the potential for higher GICs (Kelbert, 2019, Bailey et al., 2017). The geology of the region influences the resistivity of the Earth (reciprocal of conductivity), which can be obtained from Earth conductivity models. Figure 3.3 shows the EURHOM model, which is a cell-based, 1-D representation of the electrical conductivity distribution in Europe, created for the purpose of assessing the risk of geoelectric induction that may affect the electrical grid and communication systems (A. Ádám, 2012). The section covering Germany consists of 12 cells, each containing 2 to 6 horizontal

layers. The thickness of the layers ranges from 0.9 to 190 km and they cover a depth of 12 to 202 km. The layer resistivities range from 0.5 to 10,000 Ωm.

In that sense, although space weather events are the primary source of GICs and pose a threat to power systems and other technological systems on Earth, it is not just the strength of a geomagnetic storm that determines the GIC risk. In the next section it is discussed how GICs affect the power grid systems.

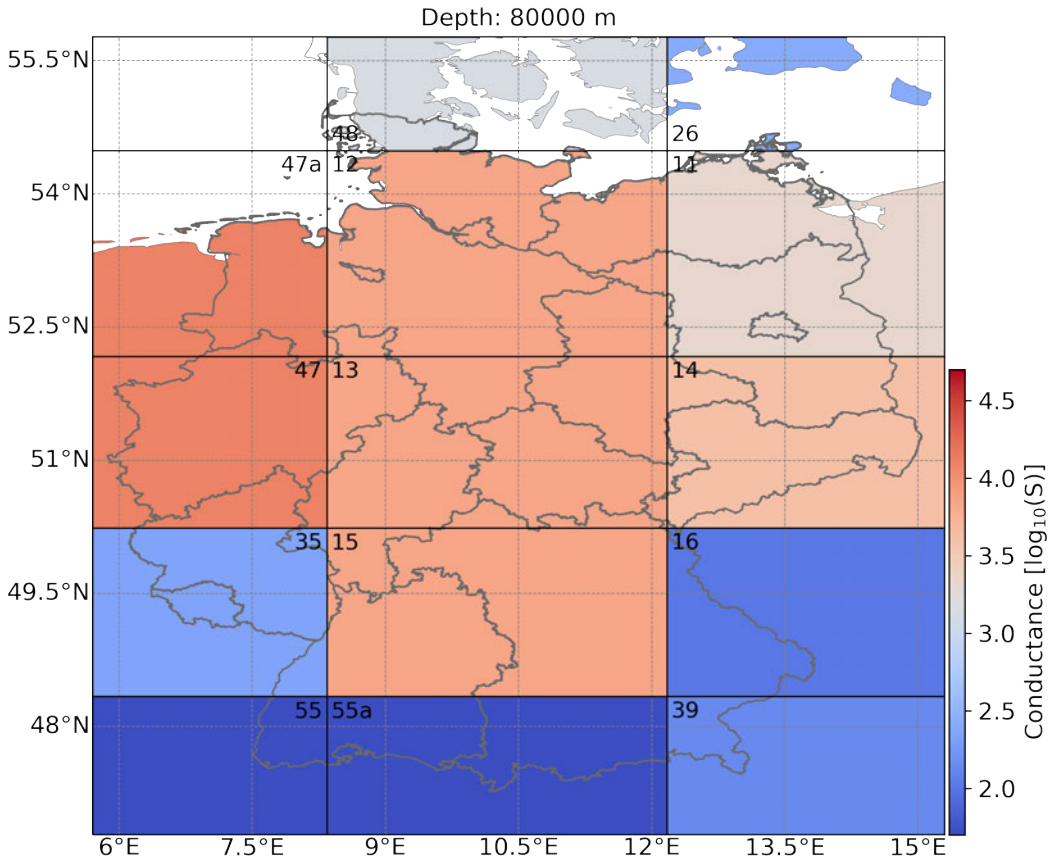

Figure 3.3: Depth-integrated conductivity (surface down to 8 km) in Germany according to EURHOM 1D model. Figure provided by L. Pick (DLR).

3.1 GIC EFFECTS ON POWER SYSTEMS

As previously discussed in section 2.2.2, an additional DC current within the transformer moves its operating point to the saturation region during the positive AC cycle (Fig. 2.5). The magnetizing current is thus increased, the leakage flux outside the core is raised, and larger eddy currents appear in the core structure. The exciting current, which was assumed to be negligible compared to the rated current of the transformer, becomes much larger, and can reach up to hundreds of amperes depending on the magnitude of the GIC. Transformers can present hot spot temperatures in their windings and structural steel parts as a result. The effect can be cumulative if the transformer is exposed to GICs for a long period of

time, such as hours or days, so that the life time of the transformer is reduced and insulation loss occurs, which could lead to transformer failure.

Once the magnetizing current becomes asymmetric, harmonics are produced. Harmonics refer to sinusoidal currents with a frequency that is an integer multiple of the fundamental frequency of the system (Singh, 2007). The addition of such currents into the system results in a non-sinusoidal current flowing and, thus, the distortion of the voltage signal. The presence of harmonic currents in transformers also increases their mechanical vibrations, raising their noise level.

A further disturbance that can be triggered by harmonics is the false operation of protection relays. The protection system is designed to detect fault conditions in order to disconnect the affected equipment from the grid and prevent it from producing greater damage. The presence of harmonics generated by GMD events, however, can result in the incorrect operation of protection relays, and grid components such as transformers, shunt capacitor banks, and static var compensators (SVCs). Removing such equipment from the grid can result in grid overload and can have a chain of tripping events as a reaction, ultimately leading to voltage instability.

Moreover, the reactive power demand in the system is increased with the higher magnetization current, and therefore the system voltage decreases, which can result in voltage instability. In extreme cases, a system collapse may follow, leading to a blackout.

The effects of GICs on the power grid are further detailed in section 2.4.2 of Halbedl, 2019. As discussed above, GMD events can lead to a cascading chain of problems, which can be summarized as: harmonics added to the system; hot spots in transformers, with permanent damage in the worst cases; unwanted relay tripping; increased reactive power demand; voltage instability; and unbalanced network, possibly resulting in a collapse of the entire system under severe conditions (Pirjola, 2007). The next section presents some of the known geomagnetic storms that are recognized to have affected the power grid in different countries woldwide.

3.2 SPACE WEATHER EVENTS

The first record of an extreme space weather event dates back to 1847, when the Carrington event occurred, resulting in GICs that caused disruptions to telegraph systems around the world. In Brussels, communication was unavailable for hours, while in Australia, a telegraph could transmit without batteries. In the northeastern US, sparks and fires were reported (Winter, 2019). Auroras could be seen at such low latitude as Colombia (Cárdenas, Sánchez, and Domínguez, 2015). The Carrington event was the most severe geomagnetic storm known so far and occurred at a time when technological systems like today's did not exist. Serving as a benchmark for space weather events, severe impacts on the electrical grid are expected should a "Carrington-like" storm were to occur today.

The Great Railway Storm occurred in May 1921, when other technological systems besides telegraph networks already existed, such as telephone and cable systems, so the effects of the GICs were more significant. In the USA, wire transmission could not take place for a day and a half. The storm caused fires at different railway

stations. In Europe, effects were also observed: a fire occurred at a telegraph station in Sweden, and in the UK, telephone and telegraph lines were interrupted (Winter, 2019).

The Hydro-Quebece 1989 outage is one of the most widely recognized storms, which had a major impact on power grids. The presence of GICs lead to harmonics generated by saturated transformers, which caused the tripping of SVCs. The absence of these devices from the electrical structure lead to system instability and large voltage fluctuations in the grid occurred, causing the tripping of five lines. The consequence was the loss of 9450 MW of generation and a 9-hour blackout across Quebec. Transformers in different other parts of Canada and the US also suffered overheating (Winter, 2019).

Thereafter, another widely recognized event followed, the Halloween Storm, which occurred from October 29 to 31, 2003. Among the many impacts caused on different technological systems, it is estimated that the blackouts resulted in economic losses of about 0.5 million US dollars. The GICs triggered a large-scale one-hour blackout in the Malmö region of southern Sweden, which interrupted the power supply to around 50,000 people (Pulkkinen et al., 2005). GIC effects were also observed in Scotland and as far as South Africa (Winter, 2019).

The storms cited above are the most extremes events known. In addition, other events were also reported. In March 1991, a storm caused the tripping of nine lines and one transformer in Sweden, while GICs of up to 130 A were recorded in the US. In November 1991, another high-voltage line tripped in Sweden due to a storm and GICs exceeding 40 A were observed in transformers in Japan (Wik et al., 2009, Kappenman, 2003). In April 2000, a transformer in Sweden experienced the highest GIC ever measured, about 300 A (Wik et al., 2009). In March 2001, a capacitor bank was triggered as a consequence of the storm in New York (Kappenman, 2003). Those are some examples of GICs recorded, between many events already observed. Although it seems that extreme events are not something usual, it is important to understand the impacts and the vulnerability of power transmission systems to such events.

This Chapter presented the chain of GICs that starts on the Sun and ends on Earth, with GICs flowing into technological systems. The problems that GICs may introduce to the power system were detailed and, in addition, extreme space weather events that have occurred in the past and an overview of the impact they caused on the operation of power grids in different regions of the world were pointed out.

4

GIC MODELING

This Chapter presents the network modeling that supports the calculation of the GICs considering the induced electric field as the starting point. The equations and details required for calculating voltages and currents in a power system with the presence of GMDs are presented, and finally, the GIC flowing in a 4-bus power system is calculated as an example.

4.1 NETWORK MODELING

The connection of the transmission lines to the Earth's surface through the neutral points of transformers creates a loop where GICs flow, as shown in Figure 3.2. As Faraday's law states, the electric field integrated around the loop is related to the magnetic flux through it. Common misconceptions about the generation of GICs include the belief that the GICs are derived from this integration. In fact, the rate of change of magnetic flux is minimal for the GIC frequencies, and it is not sufficient to produce the GICs already observed. Thus, the integral around the loop is often zero, which does not mean there is no induction. This shows, in reality, that the magnitude and direction of the electric field in the transmission line is the same as that of the electric field along the surface of the Earth (Figure 4.1; see Boteler and Pirjola, 2017).

When a geomagnetic disturbance occurs, electric currents flow in the Earth, and its resistance causes a loss of energy, which is accompanied by an IR voltage drop. An induced electromotive force (EMF) on both the Earth and the power lines will be generated by the electric field. For a uniform or layered Earth, the induced EMF in the Earth and the IR voltage drop cancel each other out, so there will be no potential gradients in the Earth and, therefore, no potential difference between the power system grounding points. In the end, only the induced EMF on the transmission lines will remain (Figure 4.1), which behaves as an additional voltage source on the power grid and drives the GIC (Boteler and Pirjola, 2017).

Thus, to model the GIC acting on a power grid, the geoelectric field induced by the geomagnetic disturbances will be added to the grid as DC voltage sources in series with the transmission lines. The DC voltage acting on a transmission line can be calculated by integrating the electric field over the path of the line as,

$$V = \int_R \vec{E}_l \cdot \vec{dl} \tag{4.1}$$

where $\vec{E}_l$ and $\vec{dl}$ are the vector geoelectric field and the vector incremental line segment along the geographic route of the line (R), respectively (Horton et al., 2012).

For a uniform electric field, it is not necessary to execute the integral and Equation 4.1 simplifies to

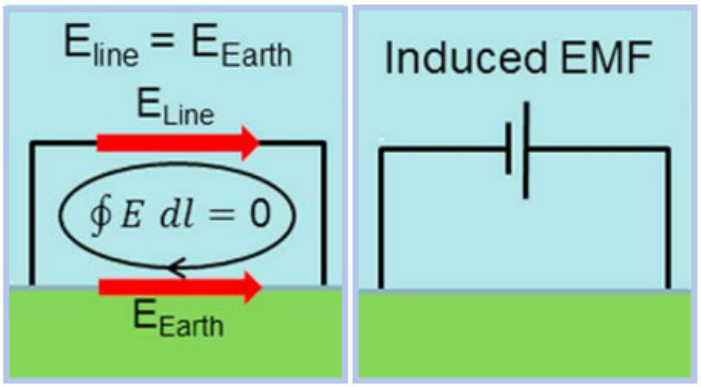

Figure 4.1: Geomagnetic induction in power systems (Boteler and Pirjola, 2017).

$$V = E_x L_x + E_y L_y, \tag{4.2}$$

where E_x and E_y denote the northward and the eastward electric field in V/m, and L_x and L_y are the northward and the eastward line length in m (Horton et al., 2012).

In reality, however, the electric field is non-uniform. Nevertheless, it is still possible to use equation 4.2 if the line is divided into small segments and the electric field over each segment is assumed to be uniform. The sum of the induced voltage calculated for each segment will then give the induced voltage over the line (Shetye and Overbye, 2019).

For the network modeling, the reactive impedances are neglected, due to the quasi-DC nature of the GICs, as already mentioned in Chapter 2. Following that, the transmission line and transformer circuit representation in Figures 2.2, 2.4 and 2.6 can be replaced by the DC equivalents in Figure 4.2 for the GIC modeling. The three-phase system is assumed to be balanced, and therefore the power grid can be modeled as a single-phase system by dividing the three-phase resistances by three (Boteler and Pirjola, 2017).

There are different approaches for solving the GIC flow model problem: the Nodal Admittance Matrix (NAM) method, the Lehtinen-Pirjola technique (Lehtinen and Pirjola), the Mesh Impedance Matrix (MIM) method and the Bus Admittance Matrix (BAM) are examples. Circuit analysis and Ohm's and Kirchhoff's laws are the basis of all methods (Marsal et al., 2022).

In this work, the NAM method is adopted. The $\boldsymbol{Y_{BUS}}$ matrix and nodal analysis equations are then formulated considering only the DC components (see equation 2.4), so that $\boldsymbol{Y_{BUS}}$ contains only conductance values. Another difference from the usual $\boldsymbol{Y_{BUS}}$ matrix is that the neutral resistances of the substations need to be included in the problem. Thus, for a system with N buses and S substations with GWye-GWye transformers, the matrix will be of size MxM, where $M = N + S$. The result is the matrix called $\boldsymbol{G}$, as for conductance matrix (Shetye and Overbye, 2019).

The next step is to include the calculated DC voltage sources to the grid. The Norton equivalent current sources can be calculated as

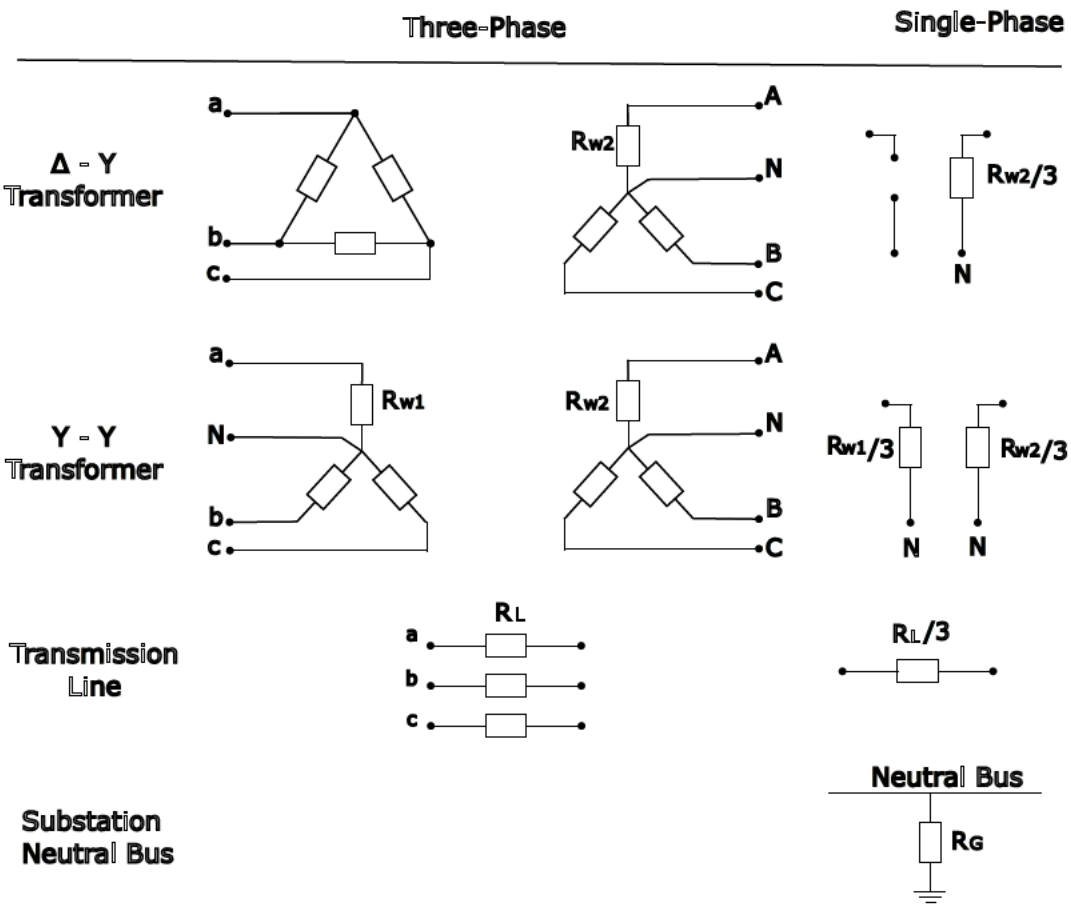

Figure 4.2: DC equivalents of power components for GIC modelling. Adapted from Halbedl, 2019

$$j = V/R_L \tag{4.3}$$

where R_L is the line resistance, and added in parallel with the line. Figure 4.3 shows an example of a power network with two voltage levels and the current source added to one line.

In order to apply nodal circuit analysis, the current injected (I_{INJ}) at each node needs to be found. According to KCL, the sum of the currents in a node (bus) is equal to zero. By convention, the currents entering a node are positive and currents leaving a node are negative. Thus, for the circuit in Figure 4.3, the current source in parallel with the line between nodes r and i can be represented by an injected current at each end of the line: one current going out of node r (-) and another current of the same amplitude going into node i (+) (Boteler and Pirjola, 2017). Subsequently, the nodal voltages can be calculated following the principle of Equation 2.5 as

$$V_n = G^{-1} I_{INJ}. \tag{4.4}$$

Once all nodal voltages are known, it is possible to find the GIC at any node. It is usually of interest to calculate the GIC at the neutral point of the transformer, since

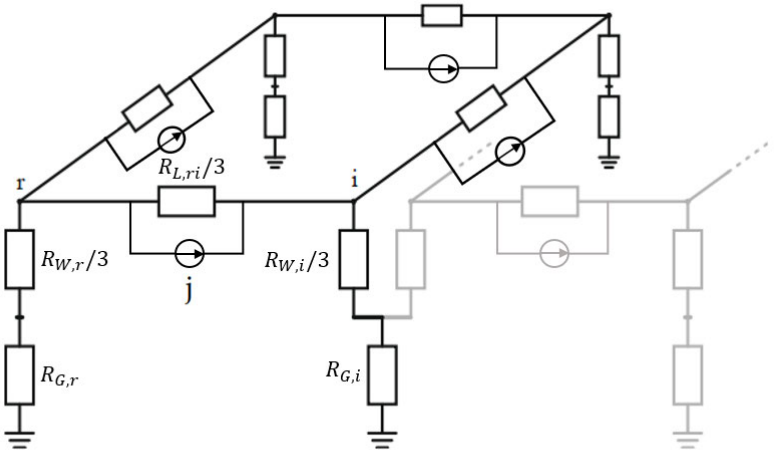

Figure 4.3: GIC induction in a power grid with two voltage levels, one represented in black and the other in grey (Halbedl, 2019).

these represent the starting point for grid problems generated by GMDs. The GIC can then be found as

$$GIC_t = G_t V_t, \tag{4.5}$$

where G_t and V_t are the conductance of the substation neutral and the voltage at the transformer neutral point.

If the electric field can be assumed spatially constant in the analyzed area, it is also possible to express the GIC at node t as a linear combination of the electric field components

$$GIC_t = a_t E_{x,t} + b_t E_{y,t}, \tag{4.6}$$

with the (unknown) coefficients a and b encapsulating the properties of transformers and power lines as well as the geometry of the network relevant to node t, given in units of $A \cdot km/V$ (Viljanen and Pirjola, 1994). When GIC measurements are available in the neutral of a transformer and the analyzed grid area is not continental, it is possible to neglect the curvature of the Earth and use plane geometry to calculate the coefficients (Torta, Marsal, and Quintana, 2014;Viljanen et al., 2012). Thus, a and b can be determined using least squares fitting. In case the configuration of the electric grid changes, the calculated coefficients are no longer valid and need to be recalculated (Albert et al., 2022).

4.2 4-BUS EXAMPLE

For the purpose of illustrating how the GIC calculation works, the 4-bus circuit in Figure 4.4 is considered.

It is assumed that an uniform electric field of $1\,V/km$ is induced along the lines and that the two lines have a length of $100\,km$. For the parameters of the lines

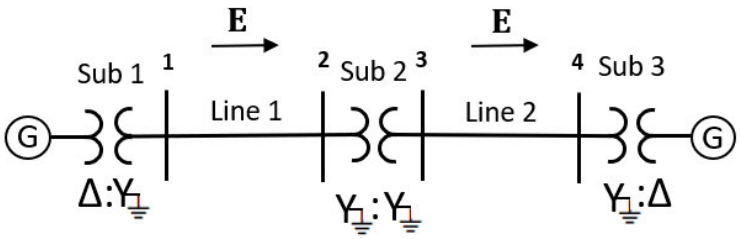

(a)

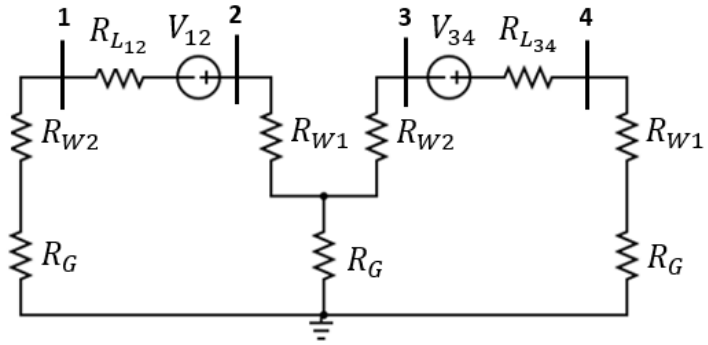

(b)

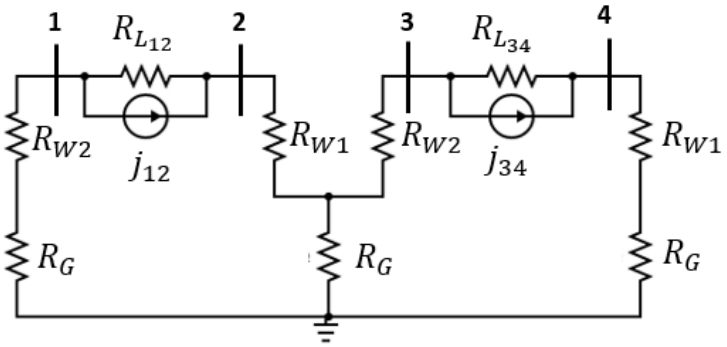

(c)

Figure 4.4: 4-bus system example. (a) is the one-line diagram. (b) and (c) consist of the system circuit representation, the first includes the induced voltages and the latter has the equivalent current sources.

and transformers, the standard values of Halbedl, 2019 and Hörsch et al., 2018 are considered, which are presented in Table 4.1. The line between buses 1 and 2 is assumed to be $380\,kV$, while the line between buses 3 and 4 is $220\,kV$.

So, in that way, the DC voltages to be added in the lines would be equal to $V_{12} = V_{34} = 1\,\frac{V}{km} \times 100\,km = 100\,V$. The resistances of the lines are $R_{L12} = 0.03\,\frac{\Omega}{km} \times 100\,km = 3\,\Omega$ and $R_{L34} = 0.06\,\frac{\Omega}{km} \times 100\,km = 6\,\Omega$ and the Norton equivalent currents can be calculated as $j_{12} = \frac{100\,V}{3\,\Omega} = 33.33\,A$ and $j_{34} = \frac{100\,V}{6\,\Omega} = 16.67\,A$. The winding resistances of transformers depend on the voltage level , so $R_{W1} = R_{W2} = 0.2\,\Omega$ and $R_{W3} = R_{W4} = 0.06\,\Omega$. The grounding resistance is the same ($R_G = 0.2\,\Omega$) for the three substations.

Table 4.1: Standard parameters for power network components.

Voltage level [kV]	**Line resistance** (R_L) [Ω/km *per phase*]	**Winding resistance** (R_W) [Ω *per phase*]	**Substation grounding resistance** (R_G) [Ω]
220	0.06	0.06	0.2
380	0.03	0.2	0.2

Since there is one trafo GWye-GWye, one additional bus should be added to its neutral. This is the bus named "5", which can be seen in Figure 4.4 (b) and (c).

Then, the matrix of conductances is constructed following Eq. 2.3,

$$G = \begin{bmatrix} \frac{1}{R_{W1}+R_G} + \frac{1}{R_{L12}} & -\frac{1}{R_{L12}} & 0 & 0 & 0 \\ -\frac{1}{R_{L12}} & \frac{1}{R_{L12}} + \frac{1}{R_{W2}} & 0 & 0 & -\frac{1}{R_{W2}} \\ 0 & 0 & \frac{1}{R_{W3}} + \frac{1}{R_{L34}} & -\frac{1}{R_{L34}} & -\frac{1}{R_{W3}} \\ 0 & 0 & -\frac{1}{R_{L34}} & \frac{1}{R_{L34}} + \frac{1}{R_{W4}+R_G} & 0 \\ 0 & -\frac{1}{R_{W2}} & -\frac{1}{R_{W3}} & 0 & \frac{1}{R_{W2}} + \frac{1}{R_G} + \frac{1}{R_{W3}} \end{bmatrix}$$

$$= \begin{bmatrix} 2.8333 & -0.3333 & 0 & 0 & 0 \\ -0.3333 & 5.3333 & 0 & 0 & -5 \\ 0 & 0 & 16.8333 & -0.1667 & -16.6667 \\ 0 & 0 & -0.1667 & 4.0128 & 0 \\ 0 & -5 & -16.6667 & 0 & 26.6667 \end{bmatrix} \tag{4.7}$$

and the $\boldsymbol{I_{INJ}}$ vector is

$$\boldsymbol{I_{INJ}} = \begin{bmatrix} -j_{12} \\ j_{12} \\ -j_{34} \\ j_{34} \\ 0 \end{bmatrix} = \begin{bmatrix} -33.33 \\ 33.33 \\ -16.67 \\ 16.67 \\ 0 \end{bmatrix} \tag{4.8}$$

Using Eq. 4.4 gives the voltage at the nodes as,

$$\boldsymbol{V_n} = \begin{bmatrix} -10.8660 \\ 7.6312 \\ 1.2279 \\ 4.2052 \\ 2.1983 \end{bmatrix} V \tag{4.9}$$

So, the GIC at the neutral of the Wye-Wye transformer can be calculated as,

$$GIC = \frac{2.1983}{0.2} = 10.9970\ A \tag{4.10}$$

The positive current means it is going into node 5. The result was verified with MATLAB Simulink.

In this Chapter, the equations for calculating the GICs flowing in an power grid have been derived from the geoelectric field that is generated by the geomagnetic activity. The $\boldsymbol{Y_{BUS}}$ matrix was modified into the $\boldsymbol{G}$ matrix to include all the resistances necessary for the GIC calculation, including the grounding resistance of substations. The calculation of the GIC at the neutral of a transformer was illustrated using a 4-bus system, including 3 transformers and 2 transmission lines. The derived equations are used for the GIC modeling in this work, which will be presented in the next Chapter, and can be applied to any power system.

5

GICS IN GERMANY

In this Chapter, the GICs are calculated for a section of the German power grid for a time period in February 2016, and the results are compared with measurements at the neutral of the transformer from Schühle and Tenbohlen, 2020. The parameters considered for the GIC modeling are analyzed, as well as their contribution to the results. In addition, a second approach to calculate GICs is conducted by performing a fit of the geoelectric field to the measurements at the transformer neutral (based on Eq. 4.6). Finally, the GICs are computed for the same power grid section using both approaches for the Halloween Storm, and the results are compared.

For the accurate modeling of the GIC flowing during real space weather events, it is necessary to consider appropriate system characteristics, magnetic fields, and the Earth conductivity structure. The work-flow in Figure 5.1 indicates the steps for calculating the GICs.

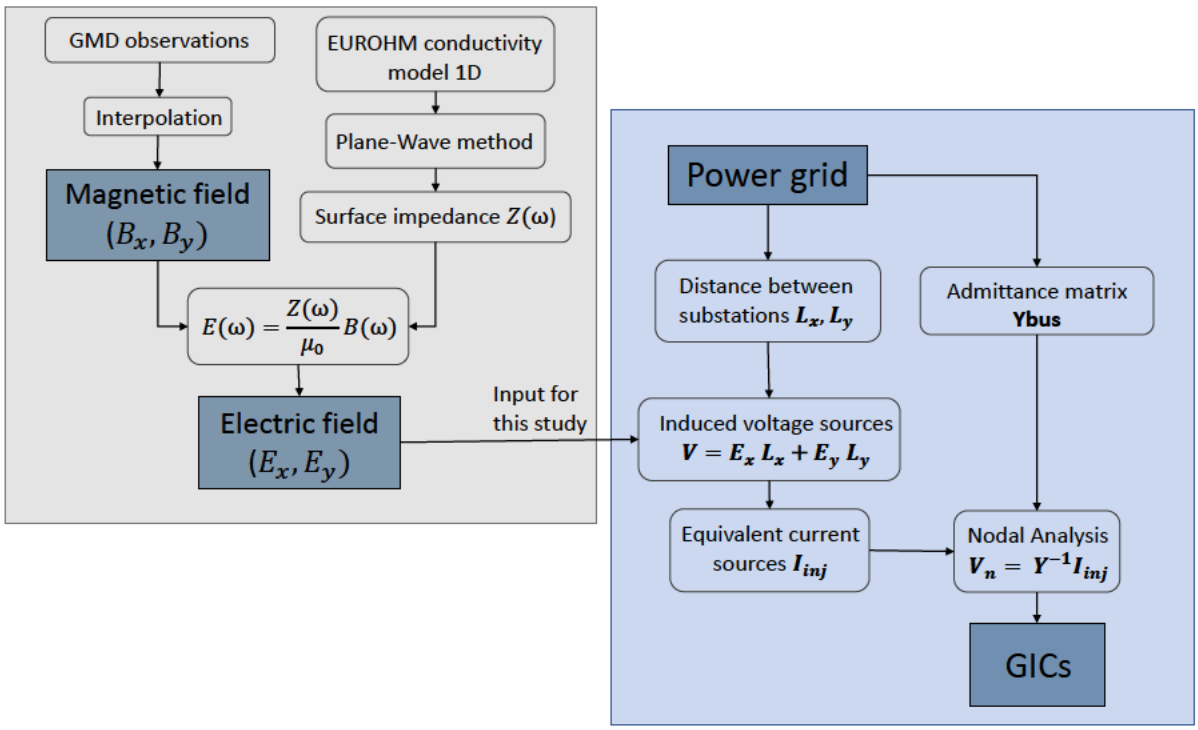

Figure 5.1: Work-flow for GIC calculation. The work-flow can be divided between: 1) the electric field calculation and 2) the GIC calculation with the electric field as input.

The grey part of the workflow in Figure 5.1 is outside the scope of this study. Magnetic field data was acquired for INTERMAGNET observatories and spatially interpolated within Germany. The coordinate system is oriented such that the X direction is north-south or latitudinal and the Y direction is east-west or longitudinal. The Z direction (vertically downwards) can be neglected in the calculation of GICs,

because at the Earth's surface, the air acts as an electric insulator, so there is no electric field component in the Z direction. The EURHOM conductivity model was used to calculate the surface impedances based on the plane-wave method, which yields the electric field from the fundamental equation of magnetotellurics. The modeled electric field (E_x, E_y) along the power lines of interest (see below) was provided by L. Pick (DLR) in the form of time series for specific time periods and used as input for the calculation of the GICs (blue part of Figure 5.1).

For modeling GICs in the German power grid, a section of the power transmission network located in the northwestern part of Germany was chosen for analysis. The motivation for this choice is that a study has already been carried out in this region (Schühle and Tenbohlen, 2020), in which GICs were modeled, and the DC current was measured at the neutral of two transformers. The results can thus be compared, and the reliability of the method implemented in this work can be tested. Figure 5.2 shows the selected power grid section. The neutral of substation C was chosen as the point of interest for the GIC calculation as it satisfies the requirement that all its connections are known (Schühle and Tenbohlen, 2020).

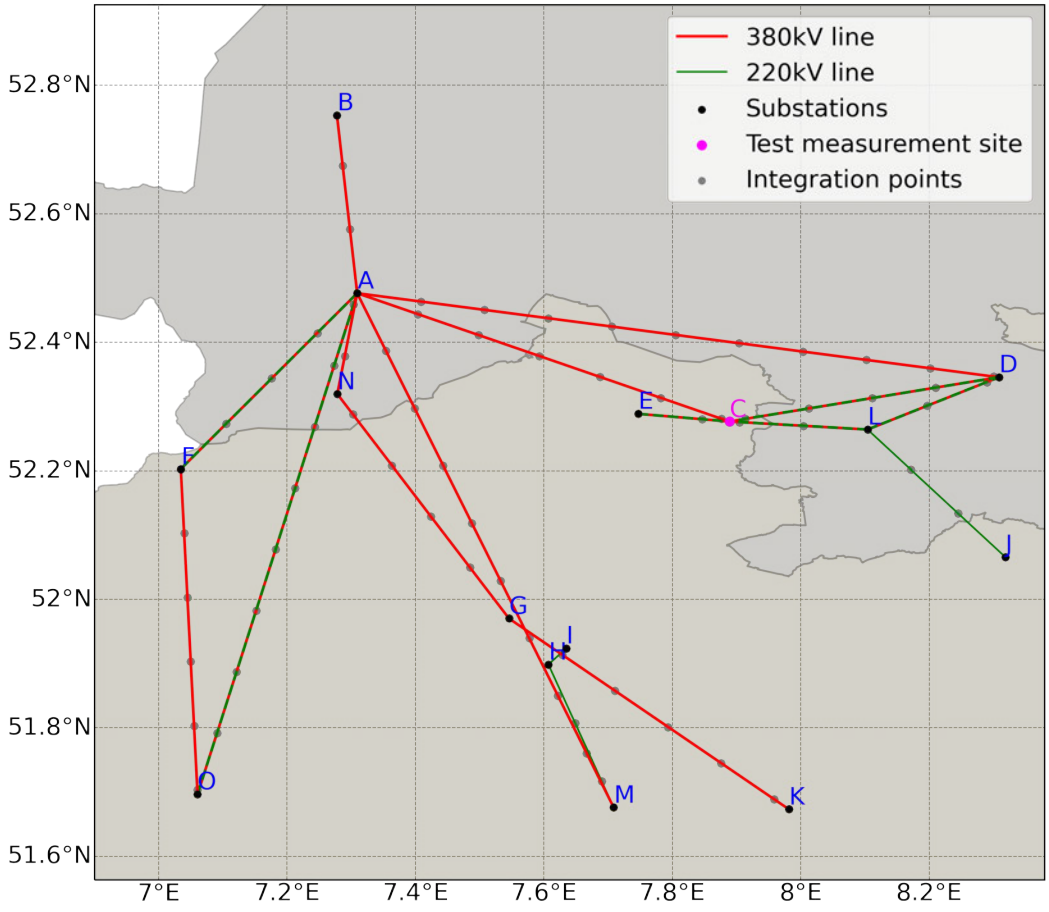

Figure 5.2: Power grid section with substations and transmission lines connections. Figure provided by L. Pick (DLR).

For the data acquisition in Schühle and Tenbohlen, 2020, the DC current at the neutral point of a GWye-GWye transformer at substation C was measured. The

measurement device relies on closed hall effect current sensors and can measure AC and DC currents in the range of $\pm 20\ A$. The recorded DC current has a cadence of 1 minute. The device was attached by linking one connector to the star point outlet of a transformer using a manual grounding rod and the other to the grounded system (Beltle, Schühle, and Tenbohlen, 2017).

As for the power grid characteristics, Table 5.1 presents the data required for calculating GICs. The German transmission operators (TSOs) publish part of their network's data, the so-called Static Network Model, which contains information about the length, connections, and electrical properties of power lines and transformers for the German power grid (JAO, 2022). The geographic location (latitude and longitude) of the substations was obtained from OpenStreetMap.

Table 5.1: Data requirement for the network modeling.

Substation	Transformer	Transmission line
name	primary and secondary winding resistance	resistance
bus connections	grounding resistance	bus connections
geographic coordinates	connection type	geographic coordinates
	nominal voltage	nominal voltage
		length

Nevertheless, not all the parameters required for modeling the GICs are known; therefore, some parameters must be assumed. For the substation grounding resistance and the winding resistances not present in the Static Network Model, the values in Table 4.1 are considered in addition to the provided actual line lengths. The distance between the substations (L_x and L_y) was calculated based on the geographic coordinates. Tables containing the information for the substations and transmission lines used for the grid configuration in Figure 5.2, as well as a schematic circuit diagram, are presented in the Appendix section.

5.1 CASE STUDY IN 2016

At first, the GIC was calculated for the same time period (February 2016) as in Schühle and Tenbohlen, 2020 for comparison of the results. Figure 5.3 shows the location of all the geomagnetic observatories considered in this study for acquiring the magnetic field data, including the location of the substation of interest (C). For the case study in 2016, the BFO, DOU, NGK, and WNG observatories were taken into account, so the same data used in Schühle and Tenbohlen, 2020 was applied. The following section will consider the other observatories illustrated in Figure 5.3. More detailed information about the observatories can be found in the Appendix section. The magnetic field in X and Y directions at each observatory is shown in Figure 5.4. For the GIC calculation, it is relevant to know the variability of the magnetic field and, for this reason, B_x - $\overline{B}_x$ and B_y - $\overline{B}_y$ (where $\overline{B}_x$ and $\overline{B}_y$ refer to the mean over the time series) are considered. Figure 5.5 presents the modeled electric field at substations C, F and L. It is noticeable that the electric field does not differ much at the different substations so that the curves overlap, except for minor

differences in the peaks that can barely be seen if the electric fields for the different substations are plotted together. A shift (+2 for substation F and +4 for substation L) has been performed to make the electric field at the different substations visible. The most intense geomagnetic variations occur within the first two days, observed in Figure 5.4, which reflects in the peaks observable in Figure 5.5.

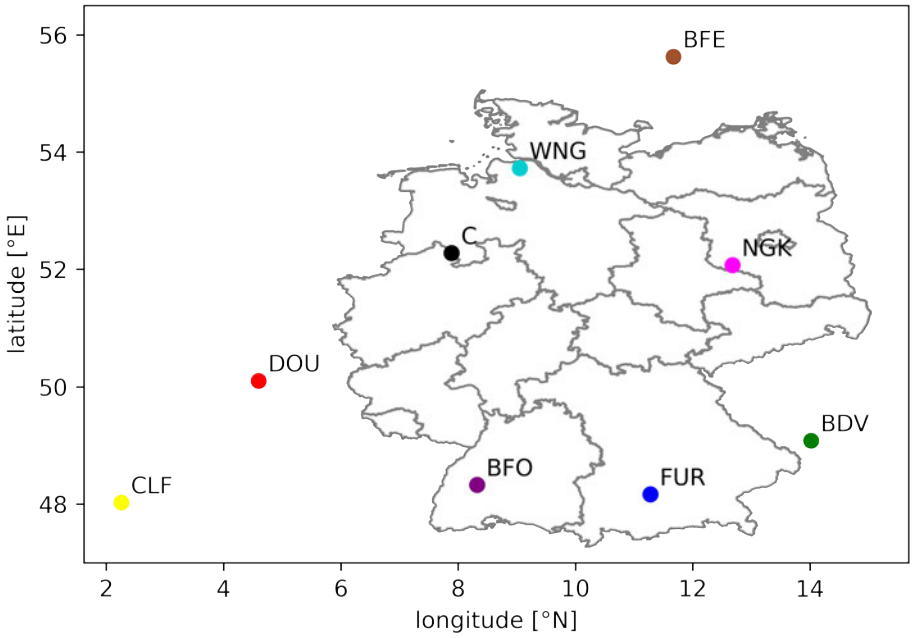

Figure 5.3: INTERMAGNET observatories and substation C (in black). Data source: INTERMAGNET, 2023.

Figure 5.6 shows the modeled GIC – or simulated GIC (GIC_s) – and the measurements (GIC_m) for the studied period of time. Comparing both curves, it is possible to see that the GIC calculated has much smaller values than the measurements, which is possibly related to the unknown parameters. Other values from the literature were then used for R_G. Table 5.2 presents the maximum absolute values calculated for the GIC over the considered time period, together with the mean and median, considering different values for the grounding resistances. It is possible to see that using $R_G = 0.1\ \Omega$ instead of $R_G = 0.2\ \Omega$ for all grounding resistances results in a GIC of higher magnitude. In all cases, the maximum value occurs at 18:28 on 2016-02-18.

From Table 5.2, it is possible to see that increasing R_G by 150% decreases the maximum GIC by approximately 32.55% (32.94% for the mean and 32.80% for the median) while decreasing R_G by 50% increases the maximum GIC by approximately 24.14% (24.66% for the mean and 24.43% for the median).

An attempt was made to decrease R_G further in order to see if there is a value for which the modeled GIC would come close to the measured curve. Non-realistic

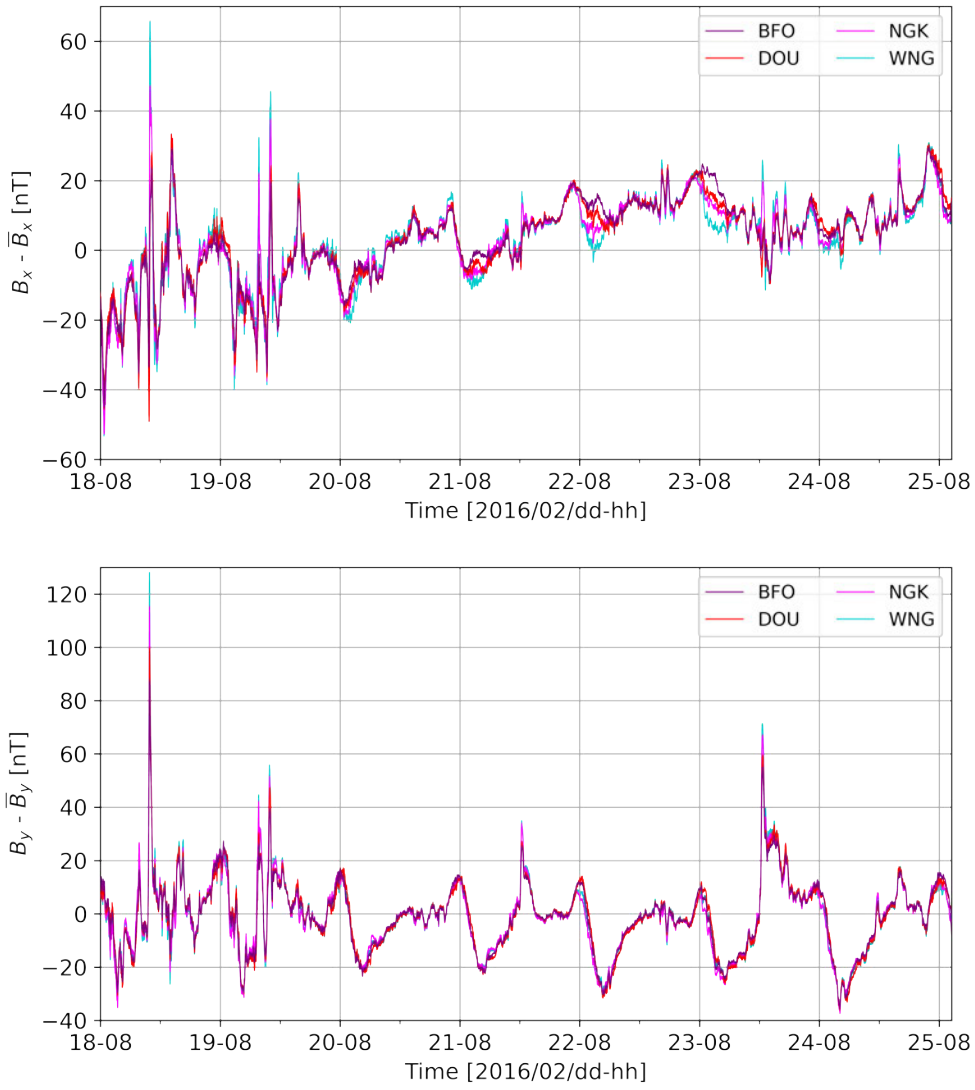

Figure 5.4: Horizontal magnetic field at the four considered INTERMAGNET observatories for the 2016 time period.

values were used, and from Table 5.3, it is possible to see that by continuing to decrease the R_G value, the GIC calculated stops increasing and becomes almost constant.

From Figure 5.7, it is possible to see that, even for a non-realistic extreme value of $R_G = 0.00001\ \Omega$, the curve for the calculated GIC remains notably different from the measurement curve. This means that other parameters need to be checked, in addition to the substation grounding resistance.

Observing the line resistances and winding resistances taken from the TSO data, it is not explicit that the values are per phase. In that sense, if the values refer to the three-phase system, they must be divided by three for the one-phase modeling. By doing so and assuming $R_G = 0.1\ \Omega$, the result is the curve in Figure 5.8.

Furthermore, it was observed that the distances calculated between the substations are smaller than the line lengths given by the Static Model from the TSO, which makes sense given that the distance calculation based on geographic points

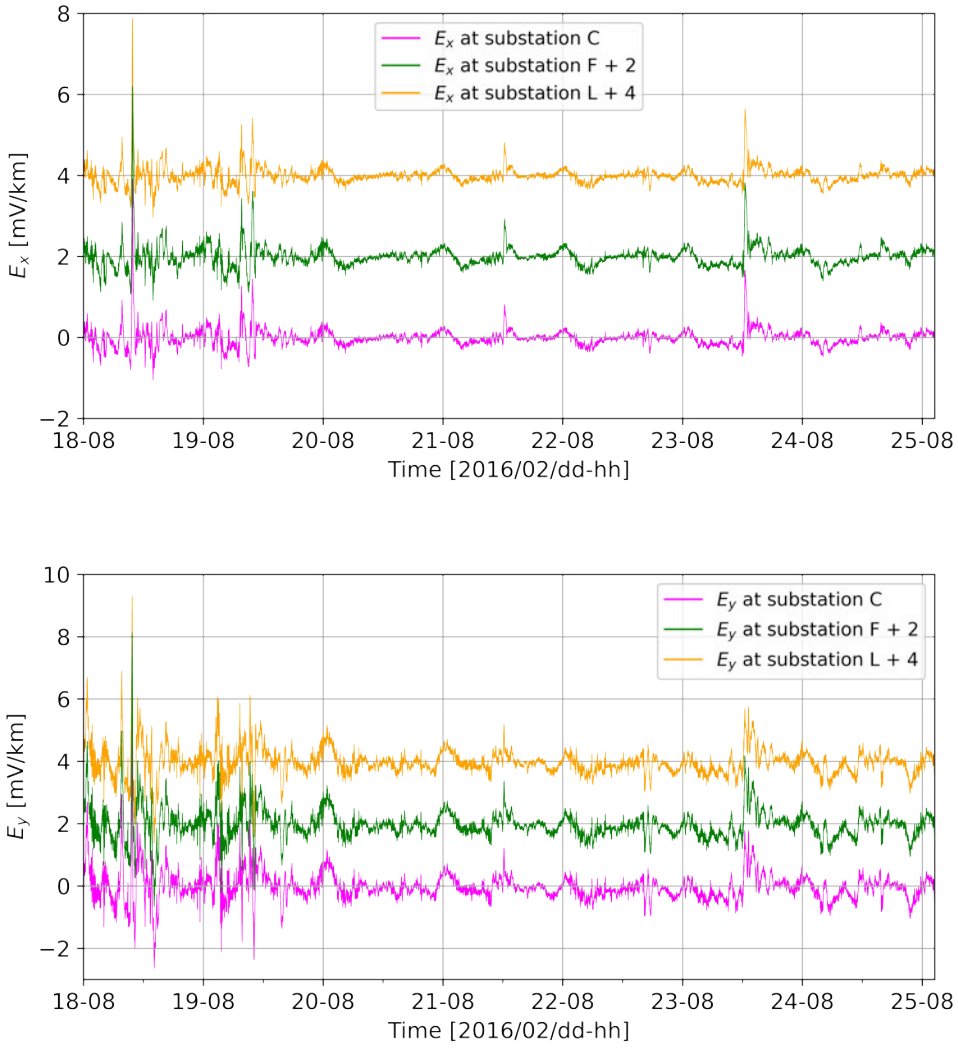

Figure 5.5: Electric field for the 2016 time period at substations C, F and L.

Table 5.2: Maximum, mean and median for absolute GIC calculated for the considered time period and different grounding resistances.

	|GIC| [A]		
R_G [Ω]	**Max**	**Mean**	**Median**
0.1	0.2980	0.0228	0.0145
0.2	0.2400	0.0183	0.0116
0.5	0.1619	0.0123	0.0078
measured	1.1147	0.0820	0.0664

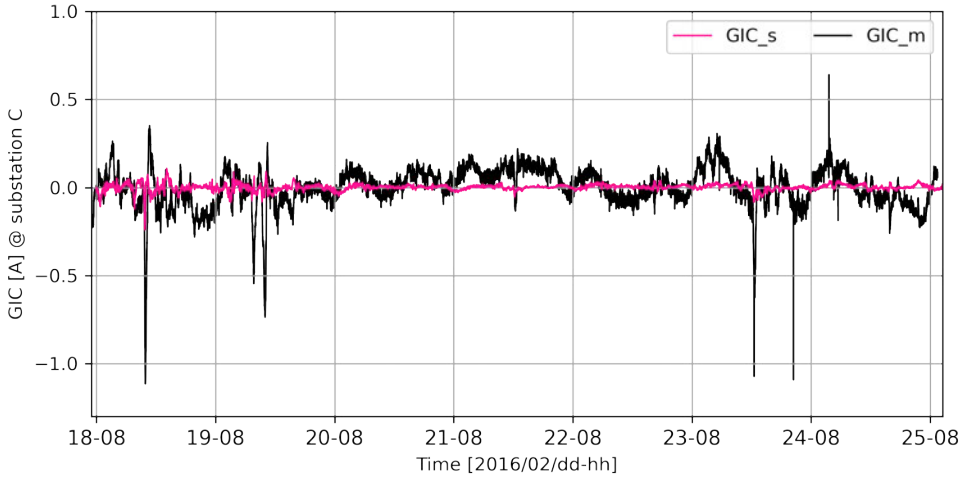

Figure 5.6: GIC at the neutral point of substation C. The measurements are shown in black (GIC_m) and the pink curve corresponds to the simulated GIC (GIC_s).

Table 5.3: Maximum, mean and median for absolute GIC calculated for the considered time period and different grounding resistances.

	|GIC| [A]		
R_G [Ω]	**Max**	**Mean**	**Median**
0.01	0.39693	0.03058	0.01935
0.001	0.41178	0.03176	0.02009
0.0001	0.41334	0.03188	0.02017
0.00001	0.41349	0.03189	0.02017
measured	1.1147	0.0820	0.0664

does not consider the routing twists and turns of the lines. The distance values (L_x and L_y) were then adjusted proportionally to be in accordance with the values provided by the TSO, as the calculation of the induced voltage directly depends on the line length (Eq. 4.2) and this affects the amplitudes of the calculated GIC. This step can be performed since the grid section does not cover such a large area that the curvature of the Earth needs to be accounted for (the longest transmission line has a length of about 100 km). Therefore, for this case, the Earth is treated as a plane for calculating the new adjusted distances L_x and L_y.

After the changes, the result is shown in Figure 5.9. It is possible to observe that the GIC calculated presents amplitudes considerably higher than in Figures 5.6 and 5.8, and closer to the measurements. Table 5.4 shows how much each step – changing the resistance of the lines and the line lengths – affects the maximum value of GIC calculated. The changes were performed for each of the considered

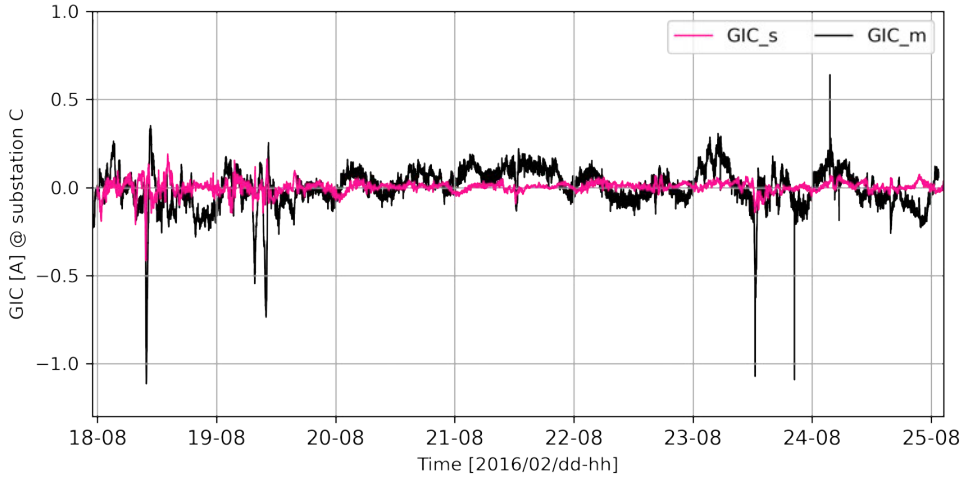

Figure 5.7: GIC at the neutral point of substation C with $R_G = 0.00001$. The measurements are shown in black (GIC_m) and the pink curve corresponds to the simulated GIC (GIC_s).

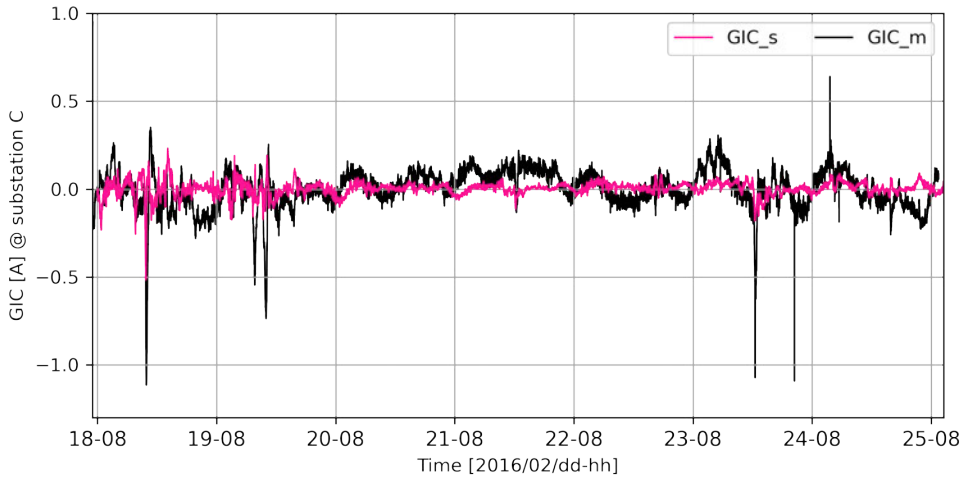

Figure 5.8: GIC at the neutral point of substation C with $R_G = 0.1\ \Omega$ and R_W and R_L from TSO divided by three. The measurements are shown in black (GIC_m) and the pink curve corresponds to the simulated GIC (GIC_s).

R_G, and the result shows that as the grounding resistance decreases, the effect of changing the other parameters increases. It is also observed that the effect of the variation of the two parameters simultaneously does not correspond to the sum of the individual effects.

The model that results in the curve in Figure 5.9 is adopted as the final model and the result for the original configuration so that the grounding resistance $R_G = 0.1\ \Omega$ is assumed, as well as the line resistances and transformer winding resistances provided by the TSO divided by three and the line lengths corrected by the factor

L/L_{calc} (L corresponds to the line length provided by the TSO and L_{calc} is the distance between two substations calculated based on the geographic coordinates).

Table 5.4: Increase provoked in the GIC median value by changing the resistance and/or the length of the lines. In relation to parameters considered in Figure 5.6.

		R_G		
		0.1	0.2	0.5
parameter changed	**multiplying factor**	**GIC median increase (%)**		
R lines	1/3	72.12	62.71	51.82
line lengths	L/L_{calc}	40.49	38.81	35.22
R and line lengths	-	139.30	120.96	98.99

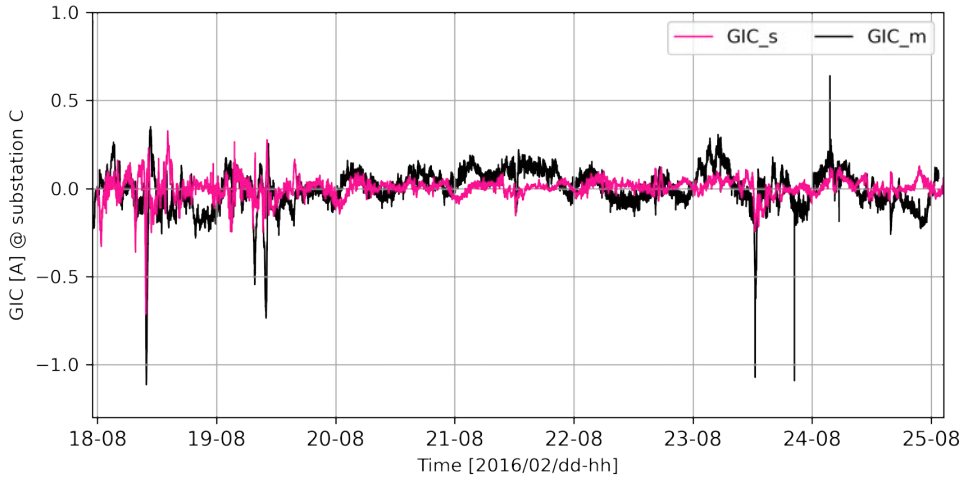

Figure 5.9: GIC at the neutral point of substation C with $R_G = 0.1\ \Omega$, R_W and R_L from TSO divided by three and line lengths corrected by factor L/L_{calc}. The measurements are shown in black (GIC_m) and the pink curve corresponds to the simulated GIC (GIC_s).

By looking at the grid area studied in Schühle and Tenbohlen, 2020, it can be seen that the grid configuration they analyze is not the same as the one derived from the TSO data at the time when this study is being conducted (Figure 5.2). Considering that the network topology greatly influences the calculation of GICs, it is also valuable to simulate scenarios in which the configuration is closer to how it was when the measurements were carried out.

In this context, two different scenarios were considered. The first (test 1) examines the same grid configuration as in Schühle and Tenbohlen, 2020. The second (test 2) comprises the current configuration (as in the TSO Static Model) with an additional transmission line observed in the test 1 configuration, which is connected between substations C and H. The last configuration was considered given that an additional line connected to substation C would have a direct impact on the GIC calculated at

its neutral point, since the presence of the line would contribute to an additional current source derived from the GMDs (Eq. 4.2 and 4.3), which would be summed to the current injected into this substation. For both tests, the additional lines were accounted for at voltage levels of 220 kV and 380 kV. Figures 5.10 and 5.11 illustrate the two tested grid configurations.

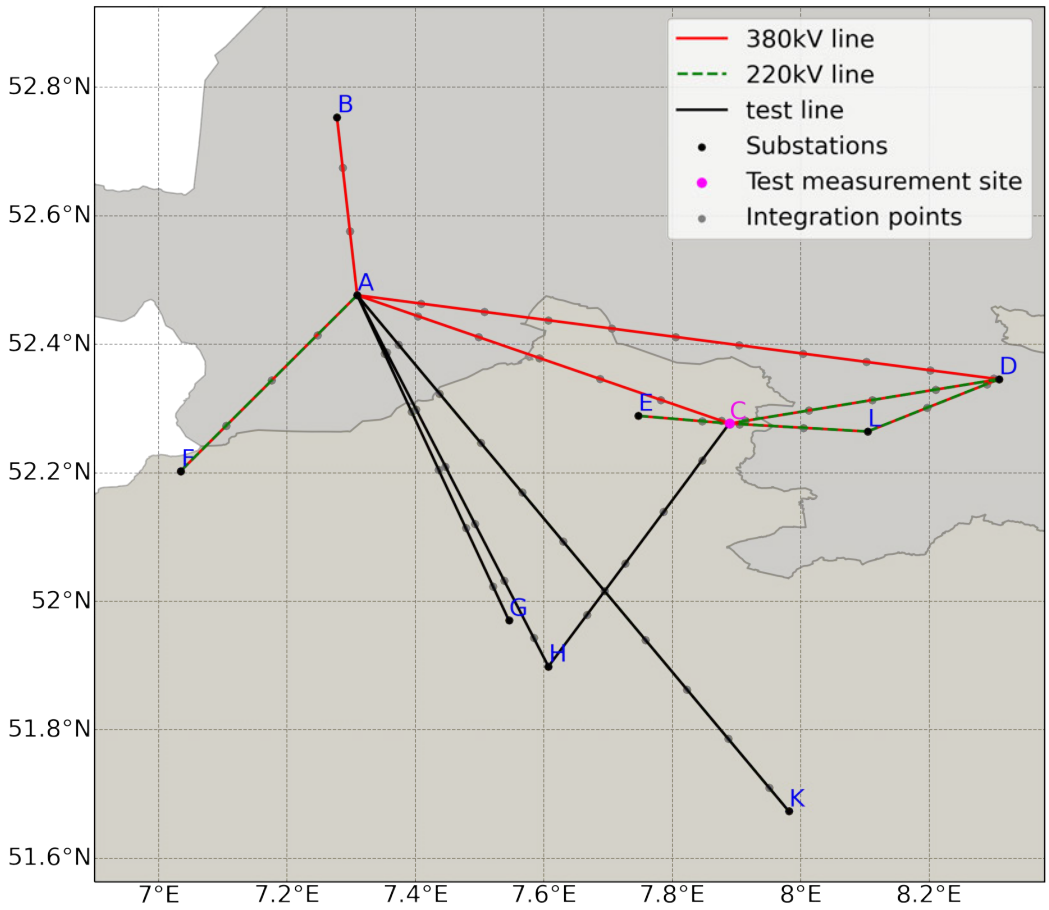

Figure 5.10: Schematic diagram for choosen grid section - test 1. Figure provided by L. Pick (DLR).

The curves presented in the upper part of Figures 5.12 and 5.13 show the modeling result for both test configurations together with the measured curve. The curves at the bottom of Figures 5.12 and 5.13 represent the difference between the modeled GIC and the original configuration (curve in Figure 5.9). It is visible that the difference is not significant, being slightly larger for test 2.

Table 5.5 displays how the peak, mean, and median of the calculated GIC's absolute value vary with the grid configuration modification. For the grid parameters considered and the configurations tested, there are no significant variations in the results.

The GIC was also calculated for other substations in the studied network area (Figure 5.2). For this, only the substations with all the connected lines presented here were taken into account, as the results are valid only for them. Figure 5.14 shows the results. The GIC is not calculated for substations with transformers

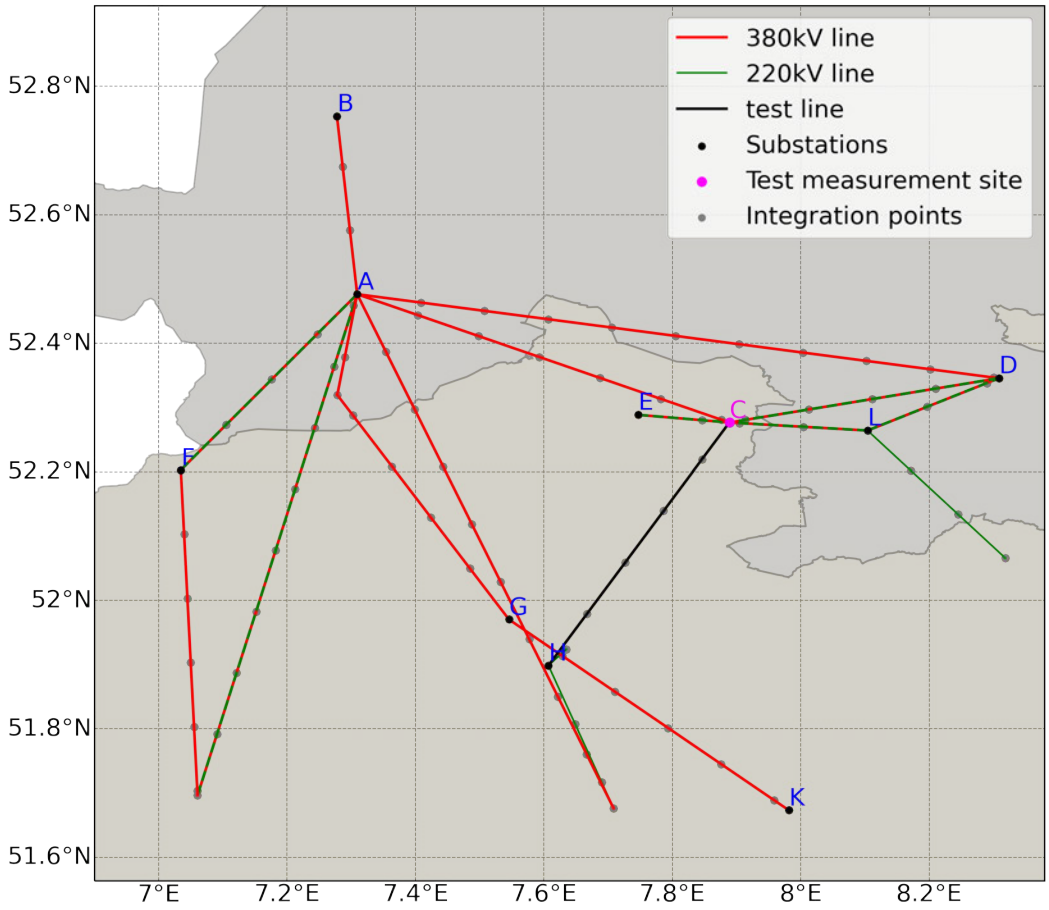

Figure 5.11: Schematic diagram for choosen grid section - test 2. Figure provided by L. Pick (DLR).

Table 5.5: Increase provoked in the peak, mean and median of absolute GIC calculated by changing the configuration of the grid. It is assumed that $R_G = 0.1\ \Omega$ and all resistances from the TSO data are divided by 3.

	|GIC| increase (%)		
	peak	**mean**	**median**
test 1	-4.81	-5.59	-5.33
test 2	4.51	2.97	2.57

assumed to have a delta side, since the presence of GICs at those substations is mitigated by the delta connection, avoiding the flow of harmonic currents into the transmission system. From Figure 5.14, it is possible to notice that the higher GIC amplitudes arise in the neutral of substation F, which are not as large as the GIC at substation C. Table 5.6 presents the maximum, mean and median of the absolute GIC values, including substation C for comparison. The GIC amplitudes at substations D, E and L are much less significant, showing that substations C and F are more susceptible to geomagnetic activity.

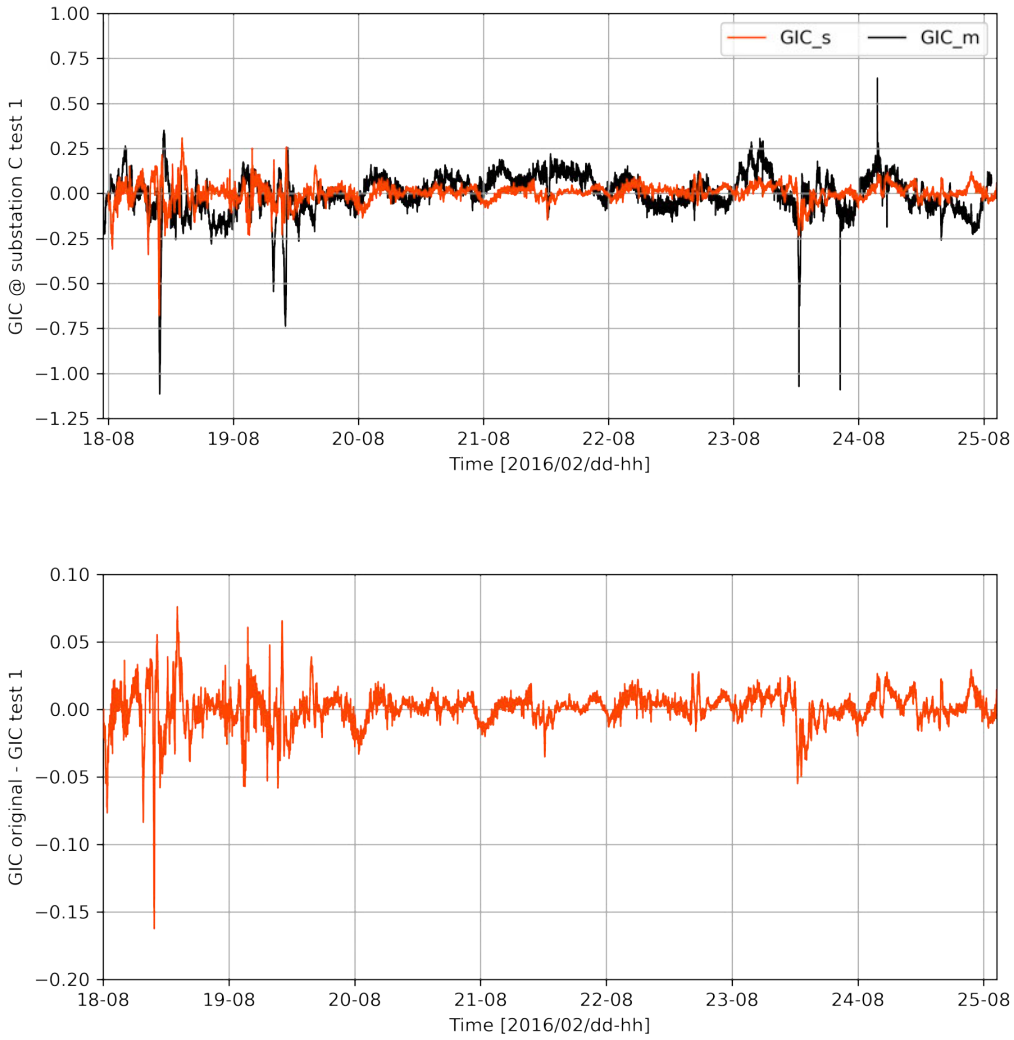

Figure 5.12: GIC at substation C for test 1.

Table 5.6: GIC at the neutral of substations C, D, E, F and L.

	|GIC| [A]		
Substation	**Max**	**Mean**	**Median**
C	0.7121	0.0548	0.0346
D	0.0710	0.0051	0.0031
E	0.1764	0.0133	0.0084
F	0.3203	0.3203	0.0137
L	0.0977	0.0059	0.0037

Furthermore, the fact that measurements at the neutral of substation C are available enables the calculation of the parameters a and b from Eq. 4.6, thus

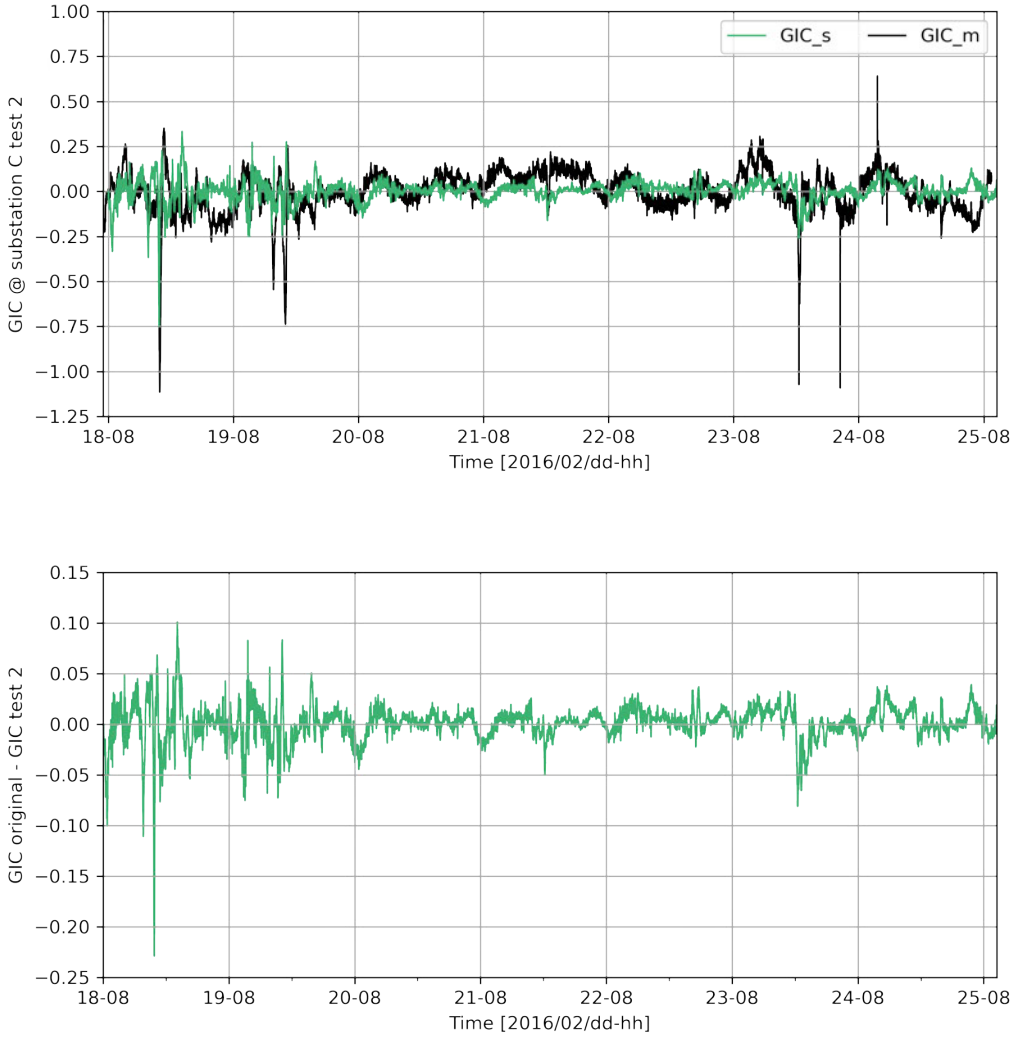

Figure 5.13: GIC at substation C for test 2.

it can be used to model GICs at different time periods. The parameters were determined using least squares fitting, resulting in $a = -65.49283055\ A \cdot km/V$ and $b = -14.73410508\ A \cdot km/V$, which are meant to describe the network configuration. Figure 5.15 shows the results of the GIC calculated based on Eq. 4.6, together with the measurements and the modeled GIC. It can be seen that, for this case scenario, the fitting does not have a good performance as a modeling approach, and the model used before performed better.

5.2 2003 HALLOWEEN STORM

Further investigation was conducted to evaluate the GICs in the studied grid area under an extreme space weather event. For this purpose, the Halloween storm of 2003 was selected. Figure 5.16 shows the magnetic field based on the

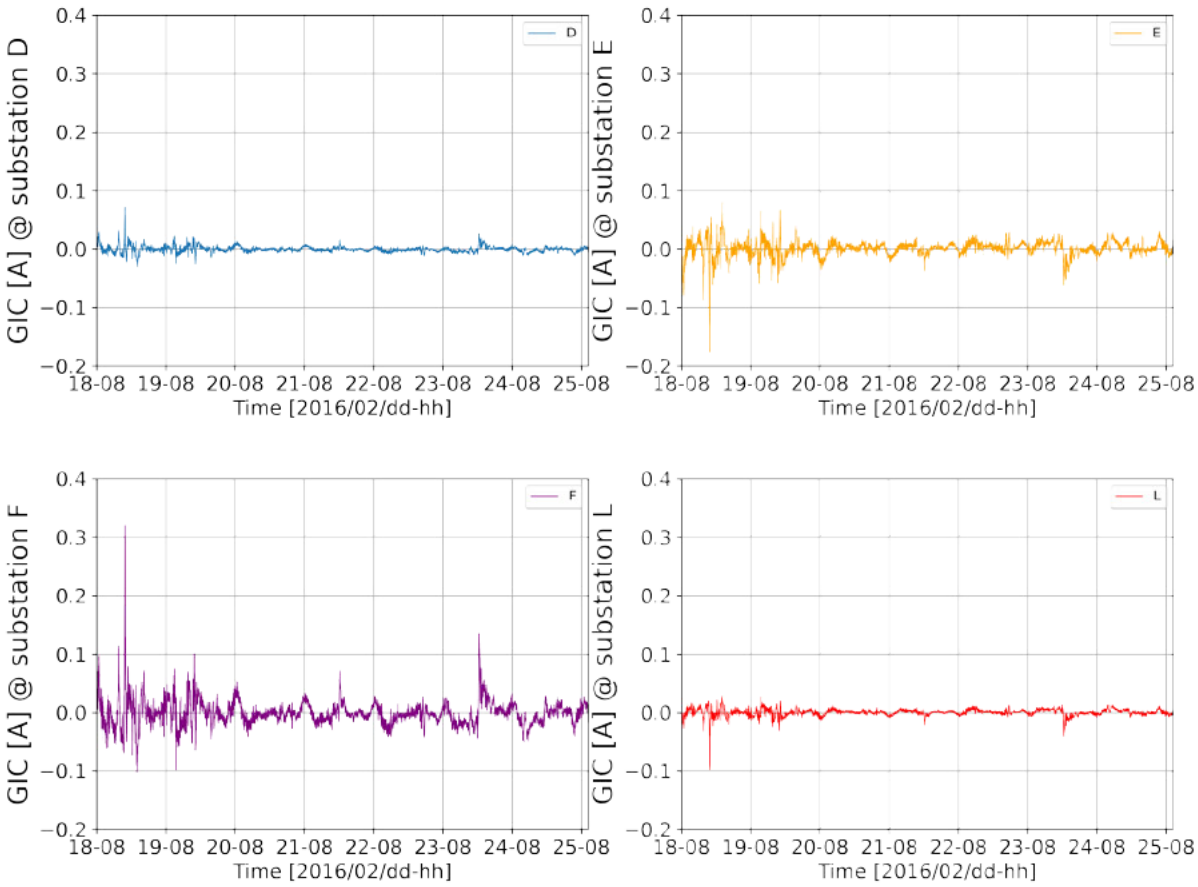

Figure 5.14: GIC at the neutral of substations D, E, F and L, from top left to bottom right.

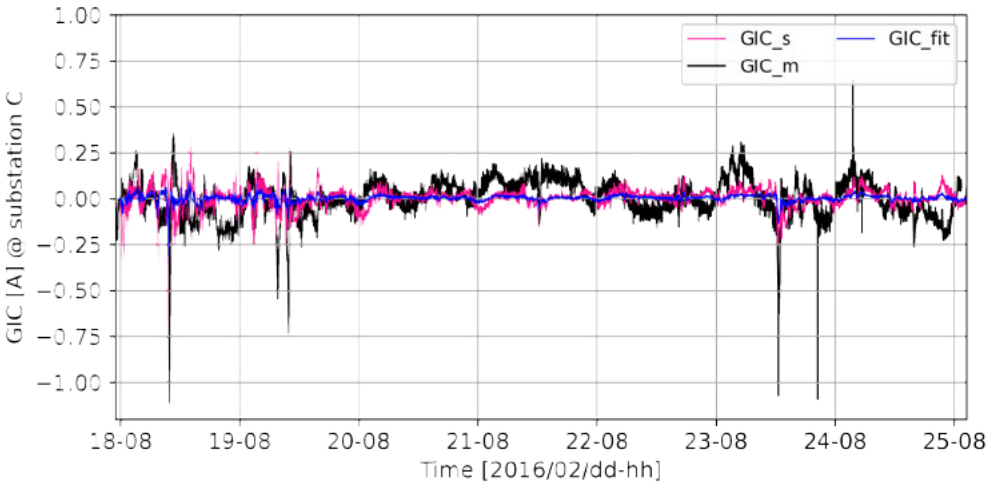

Figure 5.15: GIC at the neutral point of substation C modeled as in Figure 5.9 including fitted model. The measurements are shown in black (GIC_m), the pink curve corresponds to the simulated GIC (GIC_s) and fitted model is the blue curve (GIC_fit).

INTERMAGNET data from the observatories BDV, BFE, CLF, DOU, FUR, NGK, and WNG. Figure 5.17 presents the derived electric field at three substations.

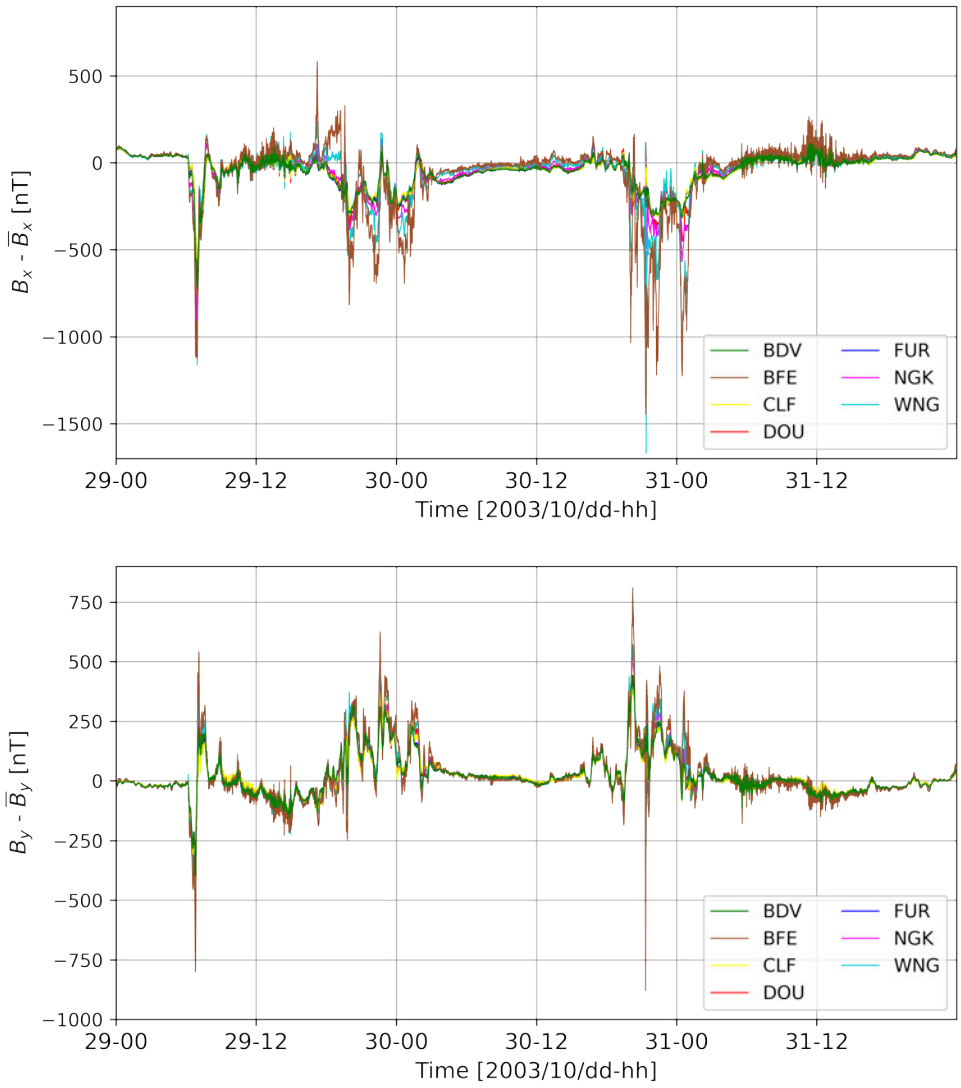

Figure 5.16: Horizontal magnetic field at the seven considered INTERMAGNET observatories during the Halloween Storm.

The GIC was calculated at the neutral point of substation C, with the result shown in Figure 5.18. The amplitudes reach over 10 A. Figure 5.19 presents the GICs modeled for substations D, E, F, and L. The behavior is the same as in the 2016 period, with the highest amplitudes (after GIC calculated at substation C) in the neutral of substation F and the lowest amplitudes calculated for substation L, as expected since the network topology remains the same. However, it is evident that the GMD affects the calculated current and dramatically increases the amplitudes so that even at substation L, the GIC reaches up to 1 A, which is close to the highest GIC amplitude for substation F in the 2016 case study.

Eq. 4.6 was applied here again for calculating the GIC at substation C based on the parameters a and b determined before. By employing the electric field displayed

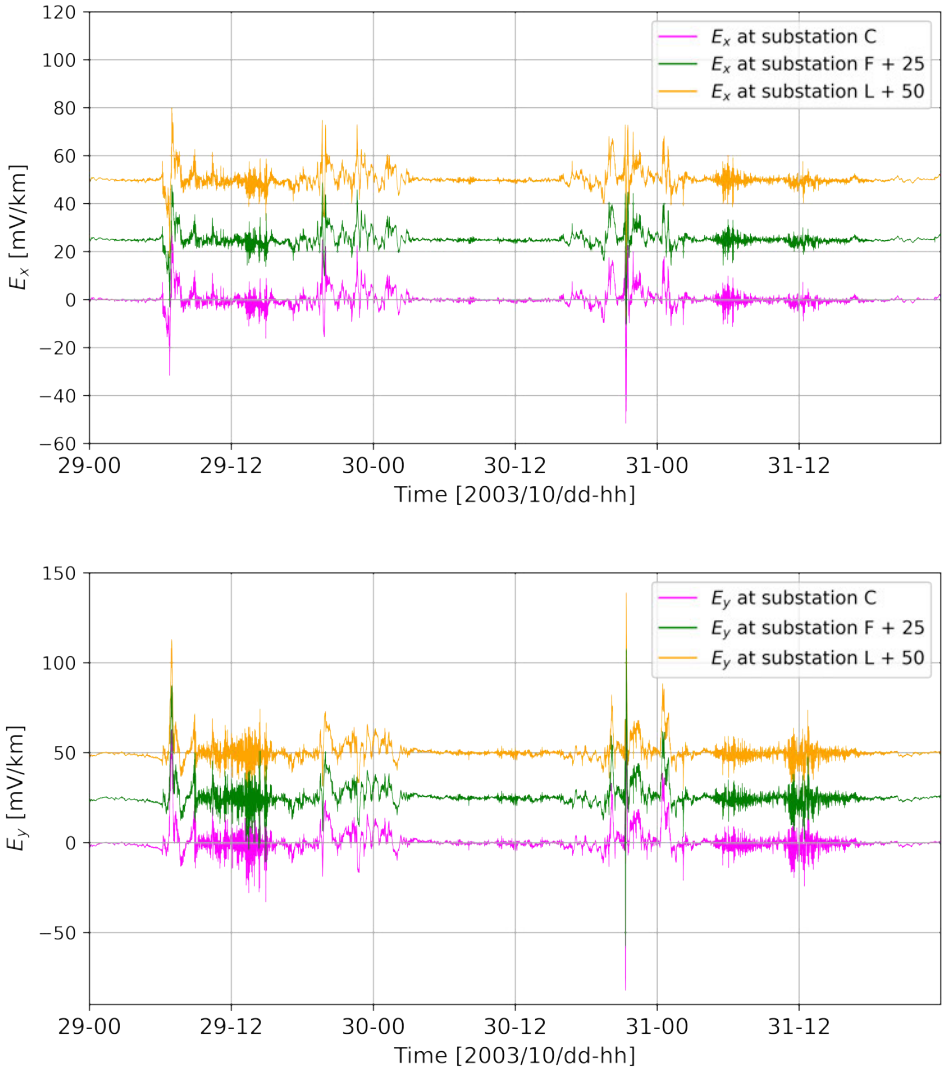

Figure 5.17: Electric field 2003 Halloween Storm in substations C, F and L.

in Figure 5.17 in Equation 4.6, the fitted model results in the blue curve presented in Figure 5.20.

From the analysis of Figure 5.20, it is evident that the blue curve follows a similar shape compared to the original model (pink), but with smaller amplitudes. The calculated parameters consider the grid in 2016, when the measurement was performed, and it is likely that the grid was different back in 2003. Therefore, updated measurements would be necessary for the fitted model to reflect the characteristics of today's grid, so the modeling based on Eq. 4.6 would be applicable today.

This chapter presented the results of the GIC modeling on a section of the power transmission grid in the northwestern part of Germany, including 15 substations and transmission lines at 220 kV and 380 kV. The results demonstrate how the network model and its electrical parameters affect the resulting GIC flowing in the neutral of the grounded transformers and how an increase of the geomagnetic activity results in much larger GICs for the same power grid. Furthermore, the

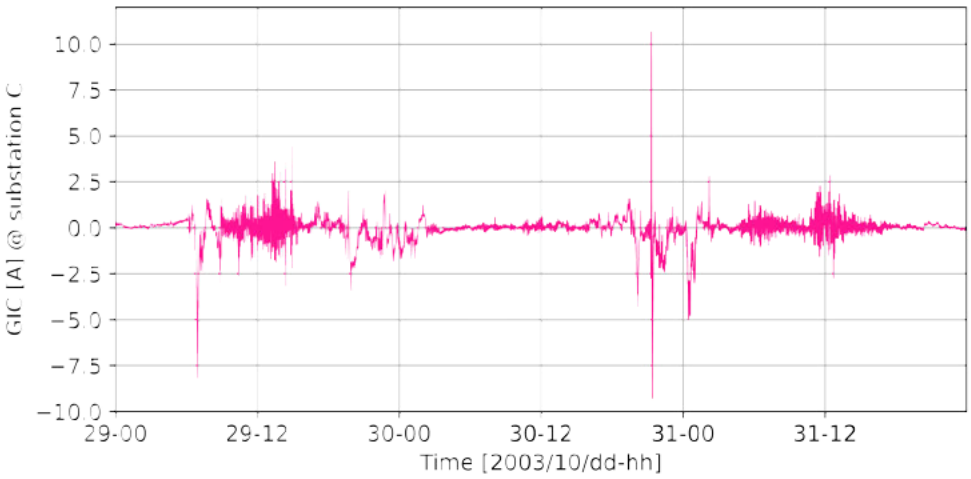

Figure 5.18: GIC at the neutral point of substation C during the Halloween Storm.

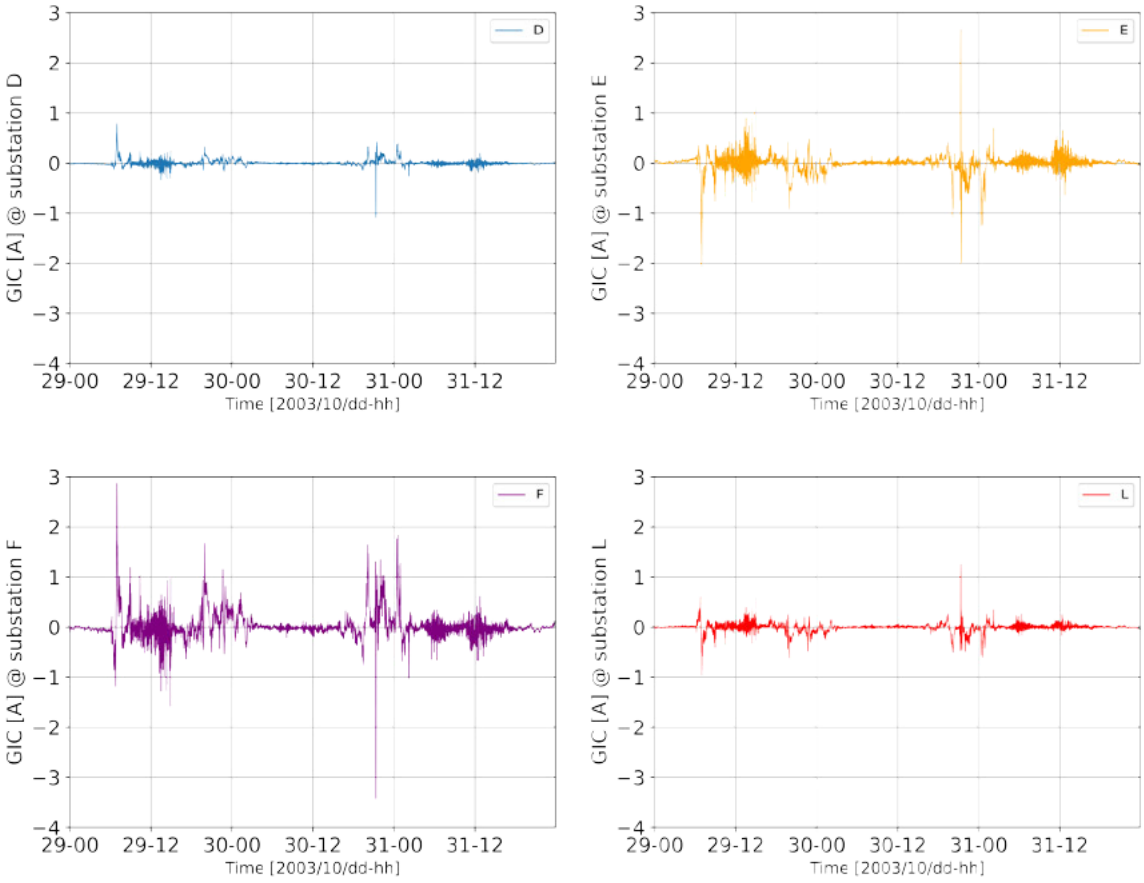

Figure 5.19: GIC at the neutral of substations D, E, F and L during the Halloween Storm, from top left to bottom right.

different models were compared to the measurements, and the modeling studied in

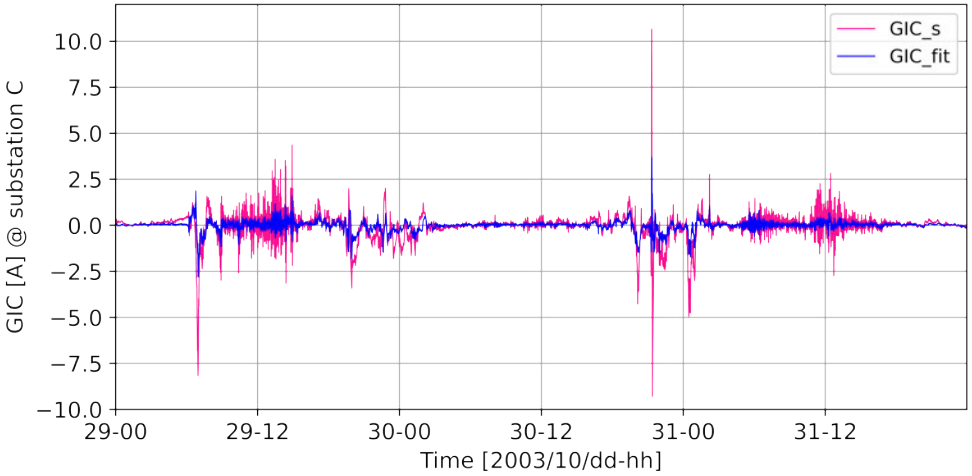

Figure 5.20: GIC at substation C for the 2003 Halloween Storm including the fitted model.

this work, accounting for the network and employing the NAM method, has shown a much better performance than the fit modeling based on Eq. 4.6.

6 DISCUSSION

Although the 2016 measurements covered a period of low geomagnetic activity, it was still possible to observe the presence of GICs in the transformer neutral. It is noticeable, however, that some of the peaks present in the measurements (between days 23 and 25) are not in the modeled curve, and it is likely that this additional current is coming from other DC sources. The original measurements had an offset (Schühle and Tenbohlen, 2020), which confirms the presence of DC sources unrelated to geomagnetic activity. Previous studies have investigated other DC sources and stated that they might originate from railway networks (Albert et al., 2022) and cathodic corrosion protection systems (Beltle, Schühle, and Tenbohlen, 2017). The GIC modeled in this work confirms that although these additional DC sources exist, geomagnetic activity is the main source for the measured DC currents in the transformer neutral.

The results also show that the grid topology plays a significant role in the GICs flowing in the grid. Regarding the sensitivity of the GICs to grid configuration and parameters, Table 5.4 indicates that line resistance is the parameter that affects the modeled GIC the most, with consideration of the parameters investigated in this work. Furthermore, it has been shown that the grounding resistance significantly contributes to the calculated GIC.

The influence of the network topology on the GICs is reinforced by comparing the results of Figure 5.14 and Table 5.6 with the electric field in Figure 5.5, since although the electric field does not show substantial variations between substations, the amplitudes of the GICs, on the contrary, have significant changes. The shape of the curves remains the same for the GICs at the different substations, following the electric field variations. The current flows in the opposite direction at substations D and F, compared to the GIC at the other substations.

It is also important to note that an additional variant plays a crucial role when modeling GICs: the geoelectric field derived from the geomagnetic field and used as input for the network modeling is modeled and can also be a source of inaccuracy for the final result. Furthermore, substation resistances are unknown for most substations, as are transformer connections (autotransformers were not considered either), and it is not known which transformers are grounded. As previously pointed out, these are essential parameters that directly affect the calculated GICs, and accurate data is necessary to achieve the best and most reliable network modeling.

Concerning the occurrence of geomagnetic storms, it is evident that the geomagnetic and geoelectric fields experienced during the Halloween Storm are much stronger than during the studied period of 2016. The consequence is that for the same modeled grid, the GICs reach much higher magnitudes (more than 10 A in the neutral of transformer C). The magnitudes, however, are not as high as that calculated in Bailey et al., 2022, where GICs reach up to 30 A in the Austrian power grid, which like Germany, is located in mid-latitude. It is important to note here that

the section of the grid studied lies in a region of relatively high soil conductivity (see Figure 3.3), which is itself a factor contributing to lower GICs. In this regard, if the scenarios studied here were performed in a region of lower conductivity, for example, in far southern Germany, GICs of higher amplitudes might be expected.

Therefore, it is of great value to evaluate the effects of geomagnetic storms in different areas of the German grid, as well as to consider larger grid sections. Further analysis would be necessary to investigate the impacts that GICs could have on the German power grid and to assess their risks.

7 CONCLUSION

This work was motivated by the lack of studies to date that provide a comprehensive understanding of the risk that GICs pose to the German high-voltage transmission network as a whole. In this context, the work carried out here is intended to serve as the first step towards assessing the hazard that extreme space weather events may represent to the German power grid. Comparing the modeling results to the measurements, it is noticeable that the model gives a good approach to reality, as even with the missing information, it reflects similar behavior and amplitudes close to the measurements. However, an analysis of the modeling results emphasizes the importance of having detailed information about the power grid characteristics. At the moment, winding resistances for all transformers, substation grounding resistances, the type of connection of the transformers, and how many and which transformers are grounded in the considered grid section are unknown. As expected, the line lengths have a significant influence on the results. How winding resistances and transformer types affect the results was not tested here and may be investigated in future work.

Comparing the GICs calculated for the Halloween storm and the GICs of the 2016 period, it is observed that during an extreme space weather event, the GICs are much higher. However, there is still the need to clarify how high the DC current in the transformer would need to be for them to cause problems in the German power grid. It is clear that geomagnetic storms are not restricted to a small area. On the contrary, they have a wide range, which means that GICs would not be limited to the area of the analyzed grid. In this sense, a further investigation of the German transmission network as a whole is necessary in order to understand the potential impacts of GMDs. It is also relevant to investigate how expanding the section of the analyzed network would affect the results.

Three factors determine whether the GIC will be high. The first is related to the geomagnetic location. Germany is a mid-latitude country, so variations in the geomagnetic field are not as high as near the poles. The second factor is related to the subsurface conductivity structure. Given that GICs are higher in areas where the ground conductivity is low, as this leads to higher geoelectric fields, it is of great interest to investigate power grids in different areas of Germany (e.g., in south-west Germany), as the section of the power grid investigated in this study is located in a region of relatively high conductivity. The third factor is the length of the transmission lines. It is worth noting that the longest line considered in this study has a length of 104 km (see Table A.2 in the Appendix section), which is relatively small compared to other transmission lines. The longest transmission line in Germany is about 230 km long (according to the Static Model). In addition, the line orientation also needs to be considered, as the GICs are larger when the line is aligned with the orientation of the geoelectric field. The model built for this

study could be used to calculate GICs for different power grids and different time periods.

Furthermore, in this work, only the DC representation of the grid components has been considered, which allows the calculation of GICs, but does not enable the analysis of how the calculated GICs would affect the power grid. For a complete analysis, the entire AC model needs to be considered, including the reactance of the power grid components, so that the full Y_{BUS} can be computed and power flow calculations can be performed. This step would be necessary for further investigations into how the GICs would impact the reactive losses and voltage stability of the system.

Finally, new measurements would be necessary to have a more reliable model by means of the fitting coefficients. It is also important to observe that if the grid configuration changes, the calculated coefficients are no longer valid, which means that new measurements would be needed every time there is a modification in the grid configuration to keep this modeling approach reliable.

A

APPENDIX

Table A.1: INTERMAGNETIC observatories. Data source: INTERMAGNET, 2023.

Observatory	Latitude	Longitude	Name	Country
BDV	49.08	14.02	Budkov	Czech Republic
BFE	55.63	11.67	Brorfelde	Denmark
BFO	48.33	8.33	Black Forest	Germany
CLF	48.03	2.26	Chambon-la-Foret	France
DOU	50.10	4.60	Dourbes	Belgium
FUR	48.17	11.28	Furstenfeldbruck	Germany
NGK	52.07	12.68	Niemegk	Germany
WNG	53.73	9.05	Wingst	Germany

Table A.2: Transmission line data referring to Figure 5.6.

Substation from	Substation to	Bus from	Bus to	Latitude from	Longitude from	Latitude to	Longitude to	Voltage [kV]	Resistance [ohm]	L [km]	Lcalc [km]	Lx [km]	Ly [km]
J	L	15	17	8.32	52.07	8.10	52.26	220	2.230	30	26.485	22.050	14.639
L	D	17	7	8.10	52.26	8.31	52.35	220	1.611	21	16.628	9.056	13.932
F	A	11	1	7.03	52.20	7.31	52.48	220	0.005	0	35.742	30.446	18.666
H	I	13	14	7.61	51.90	7.63	51.92	220	0.209	4	3.389	2.802	1.908
E	C	8	4	7.75	52.29	7.89	52.28	220	1.181	13	9.784	1.332	9.695
O	A	22	1	7.06	51.70	7.31	52.48	220	3.294	66	88.416	86.759	16.892
L	C	17	4	8.10	52.26	7.89	52.28	220	0.505	19	14.761	1.385	14.694
H	M	13	19	7.61	51.90	7.71	51.68	220	1.655	28	25.729	24.757	7.024
A	C	2	5	7.31	52.48	7.89	52.28	380	1.650	61	45.307	22.229	39.568
E	C	9	5	7.75	52.29	7.89	52.28	380	0.343	13	9.784	1.332	9.695
F	A	10	2	7.03	52.20	7.31	52.48	380	1.372	47	35.743	30.446	18.666
F	O	10	23	7.03	52.20	7.06	51.70	380	1.890	64	56.342	56.313	1.805
A	B	2	3	7.31	52.48	7.28	52.75	380	1.304	47	30.897	30.823	2.127
A	D	2	6	7.31	52.48	8.31	52.35	380	2.034	75	69.550	14.558	68.109
D	C	6	5	8.31	52.35	7.89	52.28	380	1.690	62	29.635	7.671	28.647
D	C	7	4	8.31	52.35	7.89	52.28	220	3.361	62	29.635	7.671	28.647
O	A	23	2	7.06	51.70	7.31	52.48	380	1.784	61	88.416	86.759	16.892
D	L	7	17	8.31	52.35	8.10	52.26	220	1.610	21	16.628	9.056	13.932
A	N	2	21	7.31	52.48	7.28	52.32	380	0.571	19	17.585	17.458	2.112
G	N	12	21	7.55	51.97	7.28	52.32	380	1.491	51	42.952	38.858	18.230
G	K	12	16	7.55	51.97	7.98	51.67	380	1.656	57	44.661	33.039	30.149
L	C	18	5	8.10	52.26	7.89	52.28	380	0.495	19	14.761	1.385	14.694
A	M	2	20	7.31	52.48	7.71	51.68	380	2.891	104	93.162	89.046	27.630

Table A.3: Substation data referring to Figure 5.6.

Station_ID	Trafo Type	Latitude	Longitude	Bus1	Bus2	Voltage V_1 [kV]	Voltage V_2 [kV]	Resistance R_{w1} [Ω *per phase*]	Resistance R_{w2} [Ω *per phase*]	Resistance R_G [Ω]
A	GY-GY	52.48	7.31	1	2	220	380	0.229	0.20	0.20
B	d-GY	52.75	7.28	-	3	220	380	0.06	0.20	0.20
C	GY-GY	52.28	7.89	4	5	220	380	0.229	0.20	0.20
D	GY-GY	52.35	8.31	6	7	380	220	0.331	0.06	0.20
E	GY-GY	52.29	7.75	8	9	220	380	0.06	0.20	0.20
F	GY-GY	52.20	7.03	10	11	380	220	0.131	0.06	0.20
G	d-GY	51.97	7.55	-	12	220	380	0.06	0.20	0.20
H	GY-d	51.90	7.61	13	-	220	380	0.06	0.20	0.20
I	GY-d	51.92	7.63	14	-	220	380	0.06	0.20	0.20
J	GY-d	52.07	8.32	15	-	220	380	0.06	0.20	0.20
K	d-GY	51.67	7.98	-	16	220	380	0.06	0.20	0.20
L	GY-GY	52.26	8.10	17	18	220	380	0.06	0.20	0.20
M	GY-GY	51.68	7.71	19	20	220	380	0.117	0.20	0.20
N	d-GY	52.32	7.29	-	21	220	380	0.06	0.20	0.20
O	GY-GY	51.70	7.06	22	23	220	380	0.06	0.20	0.20

Table A.4: Transmission line referring to Figure 5.9

Substation from	Substation to	Bus from	Bus to	Latitude from	Longitude from	Latitude to	Longitude to	Voltage [kV]	Resistance [ohm]	L [km]	Lcalc [km]	L/Lcalc	Lx_new [km]	Ly_new [km]
J	L	15	17	8.32	52.07	8.10	52.26	220	0.743	30	26.485	1.133	24.976	16.582
L	D	17	7	8.10	52.26	8.31	52.35	220	0.537	21	16.628	1.263	11.438	17.596
F	A	11	1	7.03	52.20	7.31	52.48	220	0.002	0	35.742	0.000	0.000	0.000
H	I	13	14	7.61	51.90	7.63	51.92	220	0.070	4	3.389	1.180	3.306	2.251
E	C	8	4	7.75	52.29	7.89	52.28	220	0.394	13	9.784	1.329	1.770	12.881
O	A	22	1	7.06	51.70	7.31	52.48	220	1.098	66	88.416	0.746	64.763	12.610
L	C	17	4	8.10	52.26	7.89	52.28	220	0.168	19	14.761	1.287	1.783	18.913
H	M	13	19	7.61	51.90	7.71	51.68	220	0.552	28	25.729	1.088	26.942	7.644
A	C	2	5	7.31	52.48	7.89	52.28	380	0.550	61	45.307	1.346	29.929	53.273
E	C	9	5	7.75	52.29	7.89	52.28	380	0.114	13	9.784	1.329	1.770	12.881
F	A	10	2	7.03	52.20	7.31	52.48	380	0.457	47	35.743	1.315	40.035	24.546
F	O	10	23	7.03	52.20	7.06	51.70	380	0.630	64	56.342	1.136	63.968	2.051
A	B	2	3	7.31	52.48	7.28	52.75	380	0.435	47	30.897	1.521	46.888	3.235
A	D	2	6	7.31	52.48	8.31	52.35	380	0.678	75	69.550	1.078	15.699	73.447
D	C	6	5	8.31	52.35	7.89	52.28	380	0.563	62	29.635	2.092	16.049	59.933
D	C	7	4	8.31	52.35	7.89	52.28	220	1.120	62	29.635	2.092	16.049	59.933
O	A	23	2	7.06	51.70	7.31	52.48	380	0.595	61	88.416	0.690	59.856	11.654
D	L	7	17	8.31	52.35	8.10	52.26	220	0.537	21	16.628	1.263	11.438	17.596
A	N	2	21	7.31	52.48	7.28	52.32	380	0.190	19	17.585	1.080	18.863	2.282
G	N	12	21	7.55	51.97	7.28	52.32	380	0.497	51	42.952	1.187	46.138	21.646
G	K	12	16	7.55	51.97	7.98	51.67	380	0.552	57	44.661	1.276	42.167	38.479
L	C	18	5	8.10	52.26	7.89	52.28	380	0.165	19	14.761	1.287	1.783	18.913
A	M	2	20	7.31	52.48	7.71	51.68	380	0.964	104	93.162	1.116	99.405	30.845

Table A.5: Substation data referring to Figure 5.9.

Station_ID	**Trafo Type**	**Latitude**	**Longitude**	**Bus1**	**Bus2**	**Voltage V_1** [kV]	**Voltage V_2** [kV]	**Resistance R_{w1}** [Ω *per phase*]	**Resistance R_{w2}** [Ω *per phase*]	**Resistance R_G** [Ω]
A	GY-GY	52.48	7.31	1	2	220	380	0.0763	0.20	0.20
B	d-GY	52.75	7.28	-	3	220	380	0.06	0.20	0.20
C	GY-GY	52.28	7.89	4	5	220	380	0.0763	0.20	0.20
D	GY-GY	52.35	8.31	6	7	380	220	0.110	0.06	0.20
E	GY-GY	52.29	7.75	8	9	220	380	0.06	0.20	0.20
F	GY-GY	52.20	7.03	10	11	380	220	0.044	0.06	0.20
G	d-GY	51.97	7.55	-	12	220	380	0.06	0.20	0.20
H	GY-d	51.90	7.61	13	-	220	380	0.06	0.20	0.20
I	GY-d	51.92	7.63	14	-	220	380	0.06	0.20	0.20
J	GY-d	52.07	8.32	15	-	220	380	0.06	0.20	0.20
K	d-GY	51.67	7.98	-	16	220	380	0.06	0.20	0.20
L	GY-GY	52.26	8.10	17	18	220	380	0.06	0.20	0.20
M	GY-GY	51.68	7.71	19	20	220	380	0.039	0.20	0.20
N	d-GY	52.32	7.29	-	21	220	380	0.06	0.20	0.20
O	GY-GY	51.70	7.06	22	23	220	380	0.06	0.20	0.20

Figure A.1: Schematic diagram for choosen grid section (Figure 5.2).

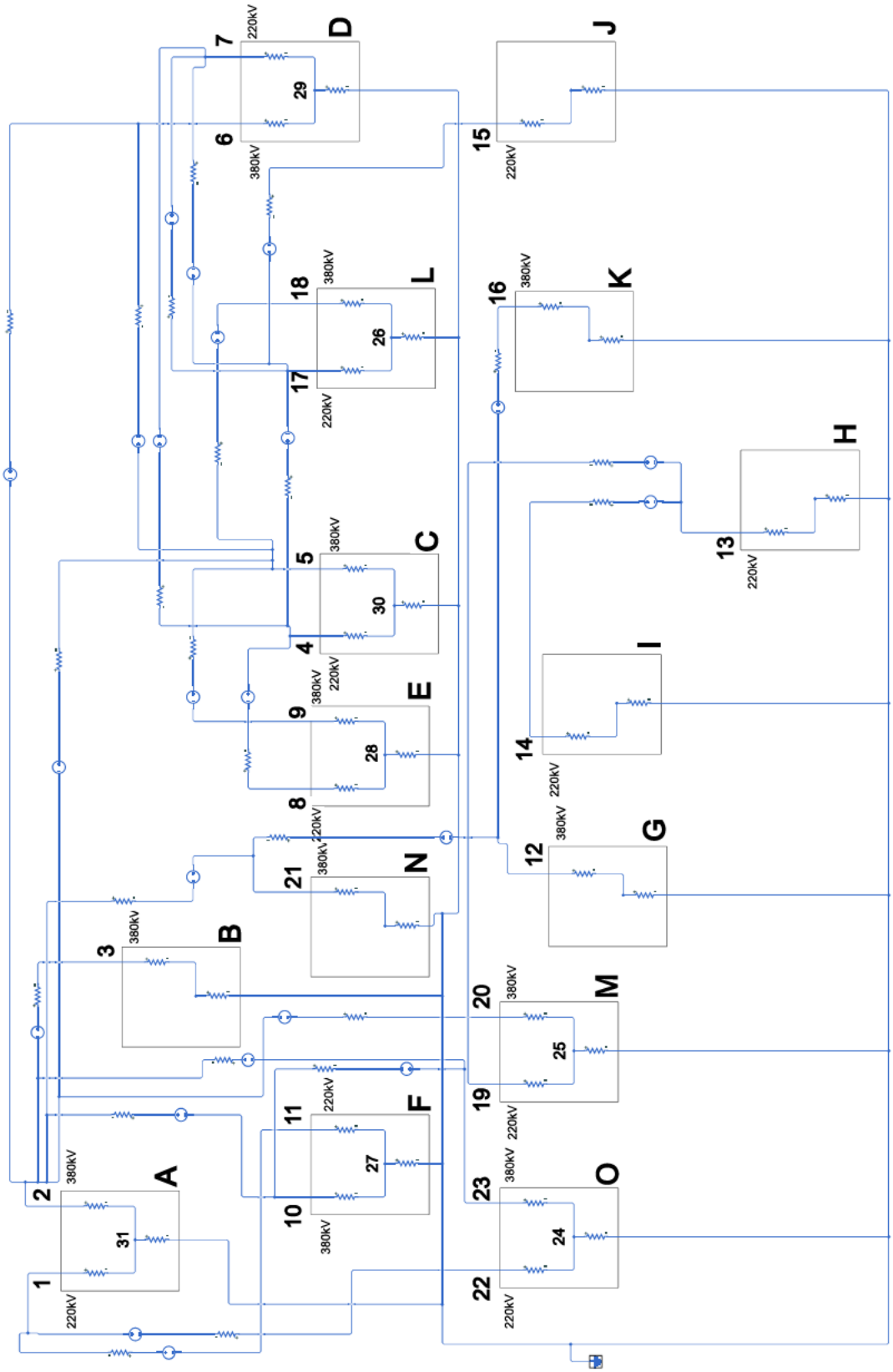

BIBLIOGRAPHY

A. Ádám E. Prácser, V. Wesztergom (2012). "ESTIMATION OF THE ELECTRIC RESISTIVITY DISTRIBUTION (EURHOM) IN THE EUROPEAN LITHOSPHERE IN THE FRAME OF THE EURISGIC WP2 PROJECT." In: *Acta Geodaetica et Geophysica* 47, 377–387. DOI: https://doi.org/10.1556/AGeod.47.2012.4.1.

Albert, D., P. Schachinger, R. L. Bailey, H. Renner, and G. Achleitner (2022). "Analysis of Long-Term GIC Measurements in Transformers in Austria." In: *Space Weather* 20.1. e2021SW002912 2021SW002912, e2021SW002912. DOI: https://doi.org/10.1029/2021SW002912. eprint: https://agupubs.onlinelibrary.wiley.com/doi/pdf/10.1029/2021SW002912. URL: https://agupubs.onlinelibrary.wiley.com/doi/abs/10.1029/2021SW002912.

Alcayde-Garcia, Francisca, Esther Salmeron-Manzano, Miguel A. Montero, Alfredo Alcayde, and Francisco Manzano-Agugliaro (2022). "Power Transmission Lines: Worldwide Research Trends." In: *Energies* 15.16. DOI: 10.3390/en15165777. URL: https://www.mdpi.com/1996-1073/15/16/5777.

Allan, Dennis and Harold Moore (2004). "Electric Power Transformer Engineering." In: ed. by James H. Harlow. CRC Press. Chap. Theory and Principles, pp. 1–12. ISBN: 978-0-203-48648-1.

Appunn, Kerstine (2021). *Ministry plans renewables expansion push to reach Germany's 2030 target*. https://www.cleanenergywire.org/news/ministry-plans-renewables-expansion-push-reach-germanys-2030-target. Last accessed January 02, 2023.

Appunn, Kerstine and Ruby Russell (2021). *Set-up and challenges of Germany's power grid*. https://www.cleanenergywire.org/factsheets/set-and-challenges-germanys-power-grid. Last accessed January 02, 2023.

Bailey, R. L., T. S. Halbedl, I. Schattauer, A. Römer, G. Achleitner, C. D. Beggan, V. Wesztergom, R. Egli, and R. Leonhardt (2017). "Modelling geomagnetically induced currents in midlatitude Central Europe using a thin-sheet approach." In: *Annales Geophysicae* 35.3, pp. 751–761. DOI: 10.5194/angeo-35-751-2017. URL: https://angeo.copernicus.org/articles/35/751/2017/.

Bailey, Rachel L., Roman Leonhardt, Christian Moestl, Ciaran Beggan, Martin Reiss, Ankush Bhaskar, and Andreas Jeffrey Weiss (2022). "Forecasting GICs and geoelectric fields from solar wind data using LSTMs: application in Austria." In: *Space Weather*. DOI: https://doi.org/10.1029/2021SW002907.

Beltle, Michael, Michael Schühle, and Stefan Tenbohlen (Aug. 2017). "Galvanic Coupling of Direct Currents in Transmission Grids and its Effects on Power Transformers." In.

Boteler, D. H. and R. J. Pirjola (Jan. 2017). "Modeling geomagnetically induced currents." In: *Space Weather* 15, pp. 258–276. DOI: https://doi.org/10.1002/2016SW001499.

Bothmer, Volker and Ioannis A. Daglis (2007). *Space Weather - Physics and Effects*. 1st ed. Springer Berlin, Heidelberg. DOI: https://doi.org/10.1007/978-3-540-34578-7.

Council, USA National Science & Technology (Mar. 2019). *NATIONAL SPACE WEATHER STRATEGY AND ACTION PLAN*. URL: https://trumpwhitehouse.archives.gov/wp-content/uploads/2019/03/National-Space-Weather-Strategy-and-Action-Plan-2019.pdf.

Cárdenas, Freddy Moreno, Sergio Cristancho Sánchez, and Santiago Vargas Domínguez (2015). "The grand aurorae borealis seen in Colombia in 1859." In: *Advances in Space Research* 57, 257–267.

DLR (2023). *Institute for Solar-Terrestrial Physics*. URL: https://www.dlr.de/so/en/desktopdefault.aspx/tabid-13420/23417_read-54014/.

Daniels, A. R. (1976). "The transformer." In: *Introduction to Electrical Machines*. London: Macmillan Education UK, pp. 43–73. ISBN: 978-1-349-15689-4. DOI: 10.1007/978-1-349-15689-4_4. URL: https://doi.org/10.1007/978-1-349-15689-4_4.

ESA (2023). *Geomagnetic Conditions Expert Service Centre (G-ESC)*. URL: https://swe.ssa.esa.int/geomagnetic-conditions.

Fang, Xi, Satyajayant Misra, Guoliang Xue, and Dejun Yang (2012). "Smart Grid ¬ The New and Improved Power Grid: A Survey." In: *IEEE COMMUNICATIONS SURVEYS & TUTORIALS* 14.4. DOI: 10.1109/SURV.2011.101911.00087.

Gannon, Jennifer L., Andrei Swidinsky, and Zhonghua Xu (2019). *Geomagnetically Induced Currents from the Sun to the Power Grid*. Ed. by Jennifer L. Gannon, Andrei Swidinsky, and Zhonghua Xu. American Geophysical Union and John Wiley & Sons, Inc.

Glover, J. Duncan, Thomas J. Overbye, Mulukutla S. Sarma, and Adam B. Birchfield (2022). *Power System Analysis & Design*. Cengage. ISBN: 978-0-357-67619-6.

Gonzalez, W. D., J. A. Joselyn, Y. Kamide, H. W. Kroehl, G. Rostoker, B. T. Tsurutani, and V. M. Vasyliunas (Apr. 1994). "What is a geomagnetic storm?" In: *JGR Space Physics* 99, pp. 5771–5792. DOI: https://doi.org/10.1029/93JA02867.

Halbedl, Thomas (2019). "Low Frequency Neutral Point Currents on Transformer in the Austrian Power Transmission Network." PhD thesis. Graz University of Technology - TU Graz.

Horton, Randy, David Boteler, Thomas J. Overbye, Risto Pirjola, and Roger C. Dugan (2012). "A Test Case for the Calculation of Geomagnetically Induced Currents." In: *IEEE TRANSACTIONS ON POWER DELIVERY* 27.4, pp. 2368–2373. DOI: 10.1109/TPWRD.2012.2206407.

Hörsch, Jonas, Fabian Hofmann, David Schlachtberger, and Tom Brown (2018). "PyPSA-Eur: An open optimisation model of the European transmission system." In: *Energy Strategy Reviews* 22, pp. 207–215. ISSN: 2211-467X. DOI: https://doi.org/10.1016/j.esr.2018.08.012. URL: https://www.sciencedirect.com/science/article/pii/S2211467X18300804.

INTERMAGNET (2023). *International Real-time Magnetic Observatory Network*. URL: https://intermagnet.github.io/.

JAO, Joint Allocation Office (2022). *Static Grid Model*. URL: https://www.jao.eu/static-grid-model.

Kappenman, John G. (2003). "Storm sudden commencement events and the associated geomagnetically induced current risks to ground-based systems at low-latitude and midlatitude locations." In: *SPACE WEATHER* 1.3. DOI: 10.1029/2003SW000009.

Kelbert, Anna (2019). "The Role of Global/Regional Earth Conductivity Models in Natural Geomagnetic Hazard Mitigation." In: *Surveys in Geophysics* 41, 115–166. DOI: https://doi.org/10.1007/s10712-019-09579-z.

Marsal, S., J. M. Torta, V. Canillas-Pérez, and J. J. Curto (2022). "A New Standalone Tool for DC-Equivalent Network Generation and GIC Calculation in Power Grids With Multiple Voltage Levels." In: *Space Weather* 20.3. DOI: https://doi.org/10.1029/2021SW002984. eprint: https://agupubs.onlinelibrary.wiley.com/doi/pdf/10.1029/2021SW002984. URL: https://agupubs.onlinelibrary.wiley.com/doi/abs/10.1029/2021SW002984.

McLloyd, Francis (2020). *File:Regelzonen mit Übertragungsnetzbetreiber in Deutschland.png*. https://commons.wikimedia.org/w/index.php?title=File:Regelzonen mit %C3%9Cbertragungsnetzbetreiber in Deutschland.png&oldid=506608992. Last accessed January 02, 2023.

Molinski, Tom S. (2002). "Why utilities respect geomagnetically induced currents." In: *Journal of Atmospheric and Solar-Terrestrial Physics* 64.16, pp. 1765–1778. ISSN: 1364-6826. DOI: https://doi.org/10.1016/S1364-6826(02)00126-8. URL: https://www.sciencedirect.com/science/article/pii/S1364682602001268.

Ngwira, Chigomezyo M. and Antti A. Pulkkinen (2019). "Geomagnetically Induced Currents from the Sun to the Power Grid." In: ed. by Jennifer L. Gannon, Andrei Swidinsky, and Zhonghua Xu. American Geophysical Union and John Wiley & Sons, Inc. Chap. An Introduction to Geomagnetically Induced Currents, pp. 4–13.

Pirjola, R. (2000). "Geomagnetically induced currents during magnetic storms." In: *IEEE Transactions on Plasma Science* 28.6, pp. 1867–1873. DOI: 10.1109/27.902215.

Pirjola, Ristor (2007). "Space Weather - Physics and Effects." In: ed. by Volker Bothmer and Ioannis A. Daglis. 1st ed. Springer Berlin, Heidelberg. Chap. 10, pp. 269–288. DOI: https://doi.org/10.1007/978-3-540-34578-7.

Pulkkinen, Antti, Sture Lindahl, Ari Viljanen, and Risto Pirjola (2005). "Geomagnetic storm of 29-31 October 2003: Geomagnetically induced currents and their relation to problems in the Swedish high-voltage power transmission system." In: *Space Weather* 3. DOI: https://doi.org/10.1029/2004SW000123.

Pulkkinen, Antti, Risto Pirjola, and Ari Viljanen (2007). "Determination of ground conductivity and system parameters for optimal modeling of geomagnetically induced current flow in technological systems." In: *Earth Planets Space* 59, 999–1006. DOI: https://doi.org/10.1186/BF03352040.

SWPC (2023). *SPACE WEATHER CONDITIONS*. URL: https://www.swpc.noaa.gov/.

Schönleber, Kevin, Alexandre Oudalov, Athanasios Krontiris, and Peter Lundberg (2020). "Opportunities for Embedded High-Voltage Direct Current - Evaluating the Benefits for the Legacy ac Grid." In: *ieee power & energy magazine* 18.5, pp. 58–63. DOI: 10.1109/MPE.2020.3001419.

Schühle, Michael and Stefan Tenbohlen (Oct. 2020). "Berechnung von geomagnetisch induzierten Strömen auf Basis eines dreidimensionalen Leitfähigkeitsmodells."

In: *e & i Elektrotechnik und Informationstechnik* 137, 400–405. DOI: https://doi.org/10.1007/s00502-020-00828-3.

Shetye, Komal S. and Thomas J. Overbye (2019). "Geomagnetically Induced Currents from the Sun to the Power Grid." In: ed. by Jennifer L. Gannon, Andrei Swidinsky, and Zhonghua Xu. American Geophysical Union and John Wiley & Sons, Inc. Chap. An Overview of Modeling Geomagnetic Disturbances in Power Systems, pp. 175–194. ISBN: 9781119434344.

Singh, G. K. (2007). "Power system harmonics research: a survey." In: *European Transactions on Electrical Power* 19, pp. 151–172. DOI: https://doi.org/10.1002/etep.201.

Singh, S. N. (2008). *Electric Power Generation, Transmission and Distribution*. Ed. by PHI Learning Private Limited. Second. ISBN: 978-81-203-35-203-3560-8.

Torta, Joan Miquel, Santiago Marsal, and Marta Quintana (2014). "Assessing the hazard from geomagnetically induced currents to the entire high-voltage power network in Spain." In: *Earth, Planets and Space*. DOI: https://doi.org/10.1186/1880-5981-66-87.

U.S.-Canada Power System Outage Task Force (Apr. 2004). *Final Report on the August 14, 2003 Blackout in the United States and Canada: Causes and Recommendations*.

Viljanen, A and R. Pirjola (1994). "Geomagnetically induced currents in the Finnish high-voltage power system." In: *Surv Geophys* 15, 383–408. DOI: https://doi.org/10.1007/BF00665999.

Viljanen, Ari, Risto Pirjola, Antal Ádám, Ernö Prácser, Yaroslav Sakharov, and Juri Katkalov (2012). "Continental scale modelling of geomagnetically induced currents." In: *Journal of Space Weather and Space Climate* 2. DOI: https://doi.org/10.1051/swsc/2012017.

Ward, David M. (2013). "The effect of weather on grid systems and the reliability of electricity supply." In: *Climatic Change*, 103–113. DOI: 10.1007/s10584-013-0916-z.

Wik, M., R. Pirjola, H. Lundstedt, A. Viljanen, P. Wintoft, and A. Pulkkinen (2009). "Space weather events in July 1982 and October 2003 and the effects of geomagnetically induced currents on Swedish technical systems." In: *Annales Geophysicae* 27, 1775–1787. DOI: https://doi.org/10.5194/angeo-27-1775-2009.

Winter, L. M. (2019). "Geomagnetically Induced Currents from the Sun to the Power Grid." In: ed. by Jennifer L. Gannon, Andrei Swidinsky, and Zhonghua Xu. American Geophysical Union and John Wiley & Sons, Inc. Chap. Geomagnetically Induced Currents from Extreme Space Weather Events, pp. 195–204.

Witulski, Arthur F. (1993). "Modeling and design of transformers and coupled inductors." In: *Proceedings Eighth Annual Applied Power Electronics Conference and Exposition*, pp. 589–595. DOI: 10.1109/APEC.1993.290725.

Zheng, Kuan, David Boteler, Risto J. Pirjola, Lian guang Liu, Richard Becker, Luis Marti, Stephen Boutilier, and Sebastien Guillon (Apr. 2014). "Effects of System Characteristics on Geomagnetically Induced Currents." In: *IEEE TRANSACTIONS ON POWER DELIVERY* 29.2, pp. 890–898. DOI: 10.1109/TPWRD.2013.2281191.

DECLARATION

I hereby confirm that my thesis entitled "Geomagnetically Induced Currents in the German Power Grid" is the result of my own work. I did not receive any help or support from commercial consultants. All sources and/or materials applied are listed and specified in the thesis.

Furthermore, I confirm that this thesis has not yet been submitted as part of another examination process neither in identical nor in similar form.

Neubrandenburg, May 2023

Aline Guimarães Carvalho